AD-A083 024 CHICAGO UNIV IL DEPT OF GEOPHYSICAL SCIENCES F/G 4/2
A QUASI-ONE-DIMENSIONAL CUMULUS CLOUD MODEL AND PARAMETERIZATIO--ETC(U)
NOV 79 H L KUO, W H RAYMOND F19628-77-C-0044
UNCLASSIFIED AFGL-TR-79-0272 NL

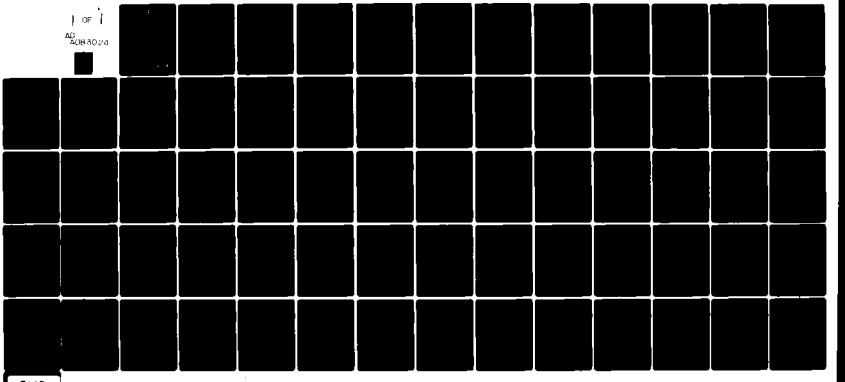

END
DATE FILMED
5-80
DTIC

AFGL-TR-79-0272

LEVEL II

12
6.5

A QUASI-ONE-DIMENSIONAL CUMULUS CLOUD MODEL AND PARAMETERIZATION OF CUMULUS HEATING AND MIXING EFFECTS

H.L. Kuo
W.H. Raymond

The University of Chicago
Office of Sponsored Programs
5801 South Ellis Avenue
Chicago, Illinois 60637

Final Report
November 1976 - September 1979

November 1979

Approved for public release; distribution unlimited

AIR FORCE GEOPHYSICS LABORATORY
AIR FORCE SYSTEMS COMMAND
UNITED STATES AIR FORCE
HANSCOM AFB, MASSACHUSETTS 01731

Unclassified
SECURITY CLASSIFICATION OF THIS PAGE (When Data Entered)

REPORT DOCUMENTATION PAGE	READ INSTRUCTIONS BEFORE COMPLETING FORM
1. REPORT NUMBER: AFGL-TR-79-0272	2. GOVT ACCESSION NO. / 3. RECIPIENT'S CATALOG NUMBER
4. TITLE (and Subtitle): A QUASI-ONE-DIMENSIONAL CUMULUS CLOUD MODEL AND PARAMETERIZATION OF CUMULUS HEATING AND MIXING EFFECTS	5. TYPE OF REPORT & PERIOD COVERED: Final Report, November 1976-September 1979 / 6. PERFORMING ORG. REPORT NUMBER
7. AUTHOR(s): H. L. KUO and W. H. RAYMOND	8. CONTRACT OR GRANT NUMBER(s): F19628-77-C-0044
9. PERFORMING ORGANIZATION NAME AND ADDRESS: Department of Geophysical Sciences, The University of Chicago, Chicago, IL 60637	10. PROGRAM ELEMENT, PROJECT, TASK AREA & WORK UNIT NUMBERS: 61102F, 2310G207
11. CONTROLLING OFFICE NAME AND ADDRESS: Air Force Geophysics Laboratory, Hanscom AFB, Massachusetts 01731, Monitor/Samuel Yee/LYD	12. REPORT DATE: November 1979 / 13. NUMBER OF PAGES
14. MONITORING AGENCY NAME & ADDRESS (if different from Controlling Office)	15. SECURITY CLASS. (of this report): Unclassified / 15a. DECLASSIFICATION DOWNGRADING SCHEDULE

16. DISTRIBUTION STATEMENT (of this Report)

Approved for public release; distribution unlimited.

17. DISTRIBUTION STATEMENT (of the abstract entered in Block 20, if different from Report)

18. SUPPLEMENTARY NOTES

19. KEY WORDS (Continue on reverse side if necessary and identify by block number)

Cumulus Convection
Cloud Model
Pressure Perturbation
Compressional Heating

20. ABSTRACT (Continue on reverse side if necessary and identify by block number)

The characteristic properties of cumulus convection are investigated using a semi-one-dimensional axisymmetric quasi-Lagrangian steady state model which takes into consideration the influences of the pressure perturbation, density stratification and nearby moist downdraft under two different environmental situations, namely, 1) a potentially more unstable tropical environment and 2) a less unstable middle latitude environment with prominent stable layers in middle troposphere. It is found that the compressional heating of the dry environment makes the cloud

DD FORM 1 JAN 73 1473 EDITION OF 1 NOV 65 IS OBSOLETE

401291

Unclassified
SECURITY CLASSIFICATION OF THIS PAGE (When Data Entered)

air warmer and reduces the updraft velocity slightly and moist downdraft cools the cloud air and reduces both the updraft and the cloud depth, while the influence of pressure perturbation is also to reduce the updraft but it is effective only for clouds of radii larger than 1000 m. The influence of density stratification is to reduce w_c slightly at low levels and augment w_c at high levels and to slightly increase the cloud depth. The calculated precipitation rates appear to be close to the representative values obtained from observations. One most interesting result given by the model is that, under the less unstable middle latitude environment, the precipitation rate jumps from lower than .7 cm/hr for cloud radii smaller than 1000 m to more than 5.4 cm/hr for cloud radii greater than 2000 m, reflecting the inhibiting effect of the mid-tropospheric stable layer on the penetrative power of the smaller clouds.

Another interesting result revealed by the model is that, with the pressure perturbation included, the maximum updraft velocity, w_{max}, achieves highest value when the cloud radius is about 8 km.

The influences of cumulus convection on the average thermodynamic properties of the atmosphere have also been calculated and it was found that the main heating is from latent heat but compressional heating of environmental air is also of importance, especially close to the top of the cloud.

An equation for the influence of vertical mixing of the horizontal momentum by cumulus convection on the change of horizontal momentum has also been obtained.

Table of Contents

1. Introduction

It is well known that the total life span of a vertically oriented thunderstorm or a single precipitating cumulus cell is only about 30 minutes and it can be divided into three distinct stages, namely, an updraft dominated developing stage, a mature or rain stage with both updraft and wet-downdraft, and a downdraft dominated dissipating stage. It is also known that the strong downdraft within the domain of the cloud itself in these systems is attributable to the downward drag created by the falling rain drops. On the other hand, the well organized, squall line type severe convective storms usually last for many hours even though the life span of a single cloud cell within the system may also be relatively short. It is evident that a very complicated model is needed if one aims at representing the various processes involved during the development of these systems in detail through numerical modeling. However, essential understanding of the mechanisms of these convective systems can be achieved by the use of much simplified models, especially when our purpose is limited to the finding of the average behaviors of these systems only.

In this study we shall at first determine the representative flow fields during the whole life spans of the cumulus clouds from a simple cloud model and then calculate the average heating effects produced by them, and finally parameterize the average heating effect in terms of the large-scale flow variables. Our approach to the cumulus parameterization problem is still as that discussed by the first author in an earlier paper (Kuo, 1974), namely, to use a representative model cloud or a

combination of clouds rather than use an unspecified cloud ensemble. This approach has also been followed by Anthes (1977) in his approach to the cumulus parameterization problem, but with a somewhat different cloud model.

Specifically, the cloud model we adopted in this study is a quasi-steady and quasi-one-dimensional model which is obtained by integrating the two-dimensional equation for the azimuthal vorticity over the radius of the cloud updraft and hence it takes into consideration the influence of the pressure perturbation approximately. In addition, we also take into consideration the influence of a nearly saturated strong downdraft in the immediate environment on the updraft in one type of cloud, which is known to occur often in nature, in addition to that with a quiescent environment only.

2. The cumulus cloud model and the governing equations

As has been mentioned in the introduction, the flow field under consideration is taken as axisymmetric and hence the radial and vertical equations of motion, the heat energy equation, the water vapor equation and the anelastic mass continuity equation can be written in the following forms in cylindrical coordinates (r,z):

$$u_t + uu_r + wu_z = -(p'/\rho_o)_r + \nu\nabla_1^2 u \quad , \tag{1}$$

$$w_t + uw_r + ww_z = -(p'/\rho_o)_z + g\left(\frac{\theta'_v}{\theta_v} - q_\ell\right) + \nu\nabla^2 w, \tag{2}$$

$$\theta'_t + r^{-1}(ur\theta')_r + \rho_o^{-1}(\rho_o w\theta')_z + w\theta_{oz} = \nu\nabla^2\theta' + L\overline{n}C/c_p, \tag{3}$$

$$q'_t + r^{-1}(urq')_r + \rho_o^{-1}(\rho_o wq')_z + wq_{oz} = \nu\nabla^2 q' - C, \tag{4}$$

$$r^{-1}(ur)_r + \rho_o^{-1}(\rho_o w)_z = 0 \quad , \tag{5}$$

where the subscripts t, r and z denote partial differentiations. Here u and w are the radial and the vertical velocity components, p', θ' and q' are the departures of the pressure p, the potential temperature θ and the water vapor mixing ratio q from their values p_o, θ_o, and q_o in the undisturbed environment, ρ_o is the undisturbed density, $\theta_v = T(1 + 0.608q)\pi$ is the potential virtual temperature, C is the rate of condensation, L is the latent heat of condensation, q_ℓ is the liquid water mixing ratio, ν is the eddy viscosity or eddy conduction coefficient, ∇^2 is the one-dimensional Laplacian operator in cylindrical coordinates and π is the ratio of the potential temperature to the temperature, which are given by

$$\nabla^2 = \frac{\partial^2}{\partial r^2} + \frac{1}{r}\frac{\partial}{\partial r} \quad , \quad \nabla_1^2 = \nabla^2 - \frac{1}{r^2} \quad , \tag{6a,b}$$

$$\pi = \left(\frac{1000}{p}\right)^{R/c_p} \quad , \qquad p \text{ in mb.} \tag{6c}$$

The undisturbed quantities p_o, θ_o, q_o and ρ_o are taken as functions of z only, and ν is taken as proportional to w in the cloud. The definitions of the symbols used in this paper are also given in the appendix.

The condensation rate in a unit mass of cloud is taken as given by the formula

$$C = -\frac{dq_s}{dt} \quad , \tag{7a}$$

where q_s is the saturation mixing ratio and is equal to q in the cloud. If all the liquid water are of the nature of small cloud drops which move with the air, then, the total water mixing ratio (q_ℓ + q) of an individual parcel without mixing or precipitation will remain constant and therefore C is also given by

$$C = \frac{dq_\ell}{dt} \quad . \tag{7b}$$

For convenience, we add $\pi L/c_p$ times (4) to (3) and obtain the following equation for the perturbation entropy s' of the moist air:

$$s'_t + r^{-1}(urs')_r + \rho_o^{-1}(\rho_o ws')_z + w\frac{\partial \hat{S}_o}{\partial z}$$
$$= \nu\nabla^2 s' + \frac{gL\pi}{c_p^2 T\bar{\theta}}(q_s - q_o)w \quad , \tag{8}$$

where

$$s' = \frac{1}{\bar{\theta}}\left(\theta' + \frac{\pi L q'}{c_p}\right) , \qquad s_o = \frac{1}{\bar{\theta}}\left(\theta_o + \frac{\pi L q_o}{c_p}\right),$$

$$\frac{\partial \hat{S}_o}{\partial z} = \frac{\partial s_o}{\partial z} - \frac{gL\pi q_o}{c_p^2 T\bar{\theta}} \quad , \tag{8a,b,c}$$

and $\bar{\theta}$ is the average value of θ_o and hence is a constant.

For the saturated region inside the cloud, it is more convenient to measure the mixing ratio perturbation from the saturation mixing ratio $q_{os} = q_s(T_o)$ at the undisturbed temperature T_o rather than from the undisturbed value q_o in the environment. Since q is equal to the saturated mixing ratio $q_s(T)$ at the temperature T (= T_o + T') in the cloud, we have

$$q = q_s(T) = q_{os} + q'' \quad , \tag{9a}$$

where

$$q'' = \frac{\partial q_s}{\partial T})_{T_o} T' = \frac{1}{\pi}\frac{\partial q_s}{\partial T})_{T_o} \theta' \quad . \tag{9b}$$

Thus, on setting $q' = q'' + q_{os} - q_o$ in s' and writing

$$s'_e = \frac{1}{\bar{\theta}}\left(\theta' + \frac{L\pi}{c_p} q''\right) = \frac{\theta'}{\bar{\theta}}\left[1 + \frac{L}{c_p}\frac{\partial q_s}{\partial T})_{T_o}\right] = s' - \frac{L\pi}{c_p\bar{\theta}}(q_{os} - q_o), \tag{9c}$$

$$s_{os} = \frac{1}{\bar{\theta}}\left(\theta_o + \frac{L\pi}{c_p} q_{os}\right) = \frac{1}{\bar{\theta}}\theta_{oes} = s_o + \frac{L\pi}{c_p\bar{\theta}}(q_{os} - q_s) \quad , \tag{9d}$$

we find that Eq. (8) becomes

$$s'_{e})_t + r^{-1}(urs'_e)_r + \rho_o^{-1}(\rho_o w s'_e)_z + w\frac{\partial \hat{S}_{os}}{\partial z}$$

$$= \nu\nabla^2 s'_e + \frac{gL\pi}{c_p^2\bar{\theta}T}(q_s - q_{os})w \quad , \tag{10}$$

where

$$\frac{\partial \hat{S}_{os}}{\partial z} = \frac{1}{\bar{\theta}}\left[\frac{d\theta_o}{dz} + \frac{L\pi}{c_p}\frac{dq_{so}}{dz}\right] = \frac{ds_o}{dz} - \frac{gL\pi q_s}{c_p^2 T\bar{\theta}} \quad . \tag{10a}$$

We apply $\partial/\partial r$ to (2) and $\partial/\partial z$ to (1) and then take their difference to obtain the following equation for the azimuthal vorticity $\eta = w_r - u_z$:

$$\eta_t + (u\eta)_r + (w\eta)_z - \nu\nabla_1^2\eta = g\frac{\partial}{\partial r}\left(\frac{\theta'_v}{\bar{\theta}_v} - q_\ell\right) \quad . \tag{11}$$

The influence of the pressure perturbation on the flow field is included in this equation through the $-u_z$ term in η.

According to Eq. (5), the velocities u and w and the vorticity η can be expressed in terms of the stream function ψ, viz.,

$$u = -\psi_z + \sigma\psi, \qquad w = \psi_r + r^{-1}\psi \quad , \tag{12a,b}$$

$$\eta = w_r - u_z = \nabla_1^2\psi - \sigma\psi_z + \psi_{zz} \quad , \tag{12c}$$

where $\sigma = -\rho_o^{-1}\frac{\partial \rho_o}{\partial z}$ is the density stratification factor. Thus the dynamics of the axisymmetric cloud can be taken as governed by the two equations (10) and (11) in terms of the two dependent variables ψ and s'_e since q_s and hence q" of (9b) is determinable from θ.

a. Equations for the cloud updraft region.

Instead of solving the equations (10) and (11) in the two-dimensional space (r,z), in this work we shall focus our attention on the cloud updraft by reducing these equations to one-dimensional forms through integration from the center of the cloud r=0 to the edge of the cloud r=R under the

assumption that we have

$$\theta'(R) = a\theta', \qquad q'(R) = b\theta'(R) = ab\theta', \tag{13a,b}$$

$$u(R) = -\alpha_1 w = -\frac{\mu}{2} Rw \quad , \tag{13c}$$

$$\int_o^R \nu r V^2 s_e' \, dr = -\alpha'' w s_e' \, , \tag{13d}$$

where a, b, α_1 and α'' are constants and θ', w and s_e' now represent their average values inside the cloud. Here $a > 0$ implies entrainment of relatively warm air, and $b > 0$ implies entrainment of air which is more moist while $b < 0$ is air drier than the undisturbed environment.

In this study we used $a = -0.1$, $b = 0.002$ for the moister downdraft and $a = 0.4$, $b = -c_p/L\pi$ for the drier downdraft. From the relations (8a), (9c) and (13a,b) we also find

$$s'(R) = \alpha' s_e' \, , \quad s_e'(R) = \alpha' s_e' - \frac{L\pi}{c_p \bar{\theta}} (q_{os} - q_o) \, , \tag{13e,f}$$

where

$$\alpha' = a(c_p + bL\pi)/(c_p + L \frac{\partial q_s}{\partial T})_{T_o}). \tag{13g}$$

We now multiply (10) by $\rho_o r dr$ and integrate over r from 0 to R. After making use of these simplifying relations at the cloud boundary we then find that the net upward transport of entropy $H(= \rho_o w R^2 s_e')$ inside the cloud is given by the following equation:

$$\frac{\partial}{\partial t} (H/w) + \frac{\partial H}{\partial z} + (\frac{\alpha''}{R^2} - \frac{\alpha^*}{R}) H =$$

$$= -M \{\frac{d\hat{s}_{os}}{dz} + \frac{L\pi}{c_p \theta} [\mu(q_{os} - q_o) - \frac{g}{c_p T} (q_s - q_{os})]\} \, , \tag{14}$$

where $M(= \rho_o w R^2)$ is the upward mass transport inside the cloud and $\alpha^* = 2\alpha_1 \alpha'$, where α' is given by (13g).

In order to be able to reduce the vorticity equation (11) to one-dimensional form in a simple manner through integration over r, we make

use of the simplifying assumption that the radial variation of ψ is oscillatory and is represented by a function of r only. For simplicity of representation, we shall follow Holton (1973) by equating this function with the first order Bessel function $J_1(\alpha r/R)$ with $\alpha = 2.405$ instead of the more realistic radial function given by the linearized equation (see Kuo, 1965b). We then have

$$\nabla_1^2 \psi \equiv \frac{\partial^2 \psi}{\partial r^2} + \frac{1}{r}\frac{\partial \psi}{\partial r} - \frac{1}{r^2}\psi = -\frac{\alpha^2}{R^2}\psi \quad . \tag{15a}$$

Since $\nabla_1^2 \psi = \frac{\partial w}{\partial r}$, this relation also implies

$$-\psi = \frac{R^2}{\alpha^2}\frac{\partial w}{\partial r} \quad . \tag{15b}$$

Thus, on making use of the relation (15b) in the $-u_z$ term of η we then find

$$\eta = [1 - \frac{R^2}{\alpha^2}(\frac{\partial^2}{\partial z^2} - \sigma\frac{\partial}{\partial z})]\frac{\partial w}{\partial r} \quad . \tag{15c}$$

Further, under the assumption that the radial and the vertical variations of w are represented by two separate functions we also find that $w\eta$ is given by

$$w\eta = \tfrac{1}{2}\frac{\partial}{\partial r}(w[w - \frac{R^2}{\alpha^2}(w_{zz} - \sigma w_z)]) \quad . \tag{15d}$$

In addition, we assume that we have

$$w(R) = 0, \quad \eta(R) = -\beta_1\bar{\eta}, \quad \int_o^R \nu\nabla^2\eta dr = -\frac{\alpha''}{R} w_o\bar{\eta} \quad , \tag{16a,b,c}$$

where w_o is the value of w at the axis and $\bar{\eta}$ is the mean value of η inside R and is given by

$$\bar{\eta} = \frac{1}{R}\int_o^R \eta dr = -\frac{1}{R}[w_o - \frac{R^2}{\alpha^2}(\frac{\partial^2 w_o}{\partial z^2} - \sigma\frac{\partial w_o}{\partial z})] \quad . \tag{16d}$$

Observe that (16c) is of the same form as (13d).

Further, we assume that the average values of w, θ_v' and q_ℓ are equal to half of their values at the center, viz.,

$$w_o = 2w_c, \quad \theta_v'(o) = 2\theta_v', \quad q_\ell(o) = 2q_\ell \quad . \tag{16e}$$

where w_c is the mean updraft velocity. Then, on integrating Eq (11) from r=0 to r=R and making use of the relations given above and setting

$$y = w_c[w_c - \frac{R^2}{\alpha^2}(\frac{d^2w_c}{dz^2} - \sigma\frac{dw_c}{dz})] \quad , \tag{16f}$$

we then find the following equation for y:

$$\frac{\partial}{\partial t}(y/w_c) + \frac{\partial y}{\partial z} + (\frac{\alpha_1'}{R} + \frac{\alpha''}{R^2})y = g\left[(1-0.5a)\frac{\theta'_v}{\theta} - (q_\ell - 0.5q_\ell(R)\right], \tag{17}$$

where $\alpha_1' = \alpha_1 r_1$. Thus the nonsteady development of our quasi-one-dimensional cloud is governed by the equations (14) and (17).

We point out that in this formulation of the problem, the flow conditions in the environment are not calculated from the dynamic equations but their influences on the flow conditions in the updraft region are included through the heat, moisture and momentum fluxes across the cloud boundary represented by (13a-d) and 16a-c) and through the second term of n in (15c) which represents the pressure effect.

b. The quasi-steady equations.

In this study we shall limit ourselves to the quasi-steady development of the cumulus convection with the removal of rain water by precipitation included but without giving rise to a downward drag on the updraft. This can be taken as possible either by assuming that the ascending current is along a slanted axis or assuming rain water is being removed from the updraft by some other process. Then the development of the cloud can be perceived as a gradual extension of the cloud top through the successive ascension of similar buoyant elements originating from the cloud base until the equilibrium level is reached, while the decay process

can be taken as accomplished statically. This kind of development can be represented by the steady versions of equations (14) and (17), namely, with the time rate of change terms omitted. For this case it is more convenient to solve for s'_e instead of the net upward entropy transport $H = Ms'_e$. Thus, on expanding dH/dz in the steady version of Eq (14) and dividing by M we then find that it reduces to

$$\frac{ds'_e}{dz} + (\mu - \frac{\alpha^*}{R} + \frac{\alpha''}{R^2})s'_e = -\frac{d\hat{S}_{os}}{dz} - \frac{L\pi}{c_p\theta}\{\mu(q_{os}-q_o) - \frac{g}{c_pT_o}(q_s-q_{os})\} \quad (18)$$

where $\mu = M^{-1}\, dM/dz = 2\alpha_1/R$ is the mass entrainment coefficient and $d\hat{S}_{os}/dz$ is given by (10a). When expressed in terms of the total equivalent potential temperature $\theta_e (= \theta + Lwq_s/c_p)$ of the saturated cloud air and when both α^* and α'' are zero, i.e., when both θ' and q' vanish at the edge of the cloud and when viscous diffusion is neglected, this equation reduces to the following simple form :

$$\frac{d\theta_e}{dz} + \mu(\theta_e - \theta_{oe}) = \frac{gL\pi}{c_pT^2}\, q_s \quad . \quad (18a)$$

It can readily be shown that, when expressed in terms of the temperature T, this equation takes the following form:

$$\frac{dT}{dz} = -\frac{(T_v + \frac{Lq_s}{R})\frac{g}{c_pT} + \mu[T-T_o + \frac{L}{c_p}(q_s-q_o)]}{(1 + \frac{0.622L}{c_p}\frac{de_s}{dT})} \quad , \quad (18b)$$

where R is the gas constant, T_v is the virtual temperature, and e_s is the saturation vapor pressure at the temperature T of the cloud. This expression of the lapse rate in the cloud is roughly equivalent to the expression given by Stommel (1947) but is slightly more general.

Since Eq. (18) can be integrated directly if we take the entrainment coefficient μ as known, we shall use this equation instead of (18a) or (18b). According to the relations (9a), (9c) and (9b), we have

$$\frac{\pi}{\theta}(q_s - q_{os}) = \frac{\partial q_s}{\partial T})_{T_o} \frac{\theta'}{\bar{\theta}} = \frac{s'_e}{\left[1+\frac{L}{c_p}\frac{\partial q_s}{\partial T})_{T_o}\right]} (\frac{\partial q_s}{\partial T})_{T_o}.$$

Therefore (18) can also be written as

$$\frac{ds'_e}{dz} + (\mu' - \frac{\alpha^*}{R} + \frac{\alpha''}{R^2})s'_e = -\frac{d\hat{S}_{os}}{dz} - \frac{L\pi\mu}{c_p\bar{\theta}}(q_{os}-q_o) \quad , \tag{19}$$

where

$$\mu' = \mu - \frac{gL}{c_p^2 T_o}\frac{\partial q_s}{\partial T}/(1 + \frac{L}{c_p}\frac{\partial q_s}{\partial T}) \quad , \tag{19a}$$

$$\frac{d\hat{S}_{os}}{dz} = \frac{1}{\bar{\theta}}\{\frac{d\theta_o}{dz} + \frac{L}{c_p}\frac{dq_{os}}{dz}\} \quad . \tag{19b}$$

Here $\partial q_s/\partial T$ is for $T=T_o$. Since all the terms on the right hand side of (19) are functions T_o and p_o, all of them are known functions of z; therefore Eq (19) can be integrated directly provided μ' is taken as known.

For q_{os} and $\partial q_s/\partial T$, we make use of the following relations:

$$q_s = \frac{0.622e_s}{p-e_s} \quad , \tag{19c}$$

$$e_s(T) = 6.11 \times \exp\{25.22\ (1 - \frac{273K}{T})\}\ (\frac{273K}{T})^{5.31} \quad . \tag{19d}$$

Thus, from these relations we find

$$\frac{\partial q_s}{\partial T} = \frac{0.622p}{(p-e_s)^2}\frac{de_s}{dT} \quad . \tag{19e}$$

The variation of the liquid water mixing ratio with height due to

condensation is calculated from a similar equation in accordance with (7a), viz.,

$$\frac{dq_{\ell\,\text{cond.}}}{dz} = -\frac{dq_s}{dz} - \mu' \{q_s - q^* + (1+a_2) q_{\ell\,\text{cond.}}\} \quad . \qquad (20)$$

where $q_{\ell\,\text{cond.}}$ refers to the total liquid water mixing ratio created by condensation and q^* is the mixing ratio at $r=R_*$ just outside the updraft and a_2 is another constant factor for allowing the effect of evaporation at the cloud boundary. The formula for calculating the rate of precipitation from the various layers will be given later in section 4. Thus our system is represented by (19) and the steady version of (17), viz.,

$$\frac{dy}{dz} + \left(\frac{\alpha_1'}{R} + \frac{\alpha''}{R^2}\right) y = g \left\{(1-0.5a)\frac{\theta_v'}{\bar{\theta}} - q_\ell + 0.5\, q_\ell(R)\right\} \quad . \qquad (21)$$

C. Two types of immediate environment.

In this paper we shall investigate the influences of two different types of immediate environment on the updraft, namely, 1) the quiescent far away environment unaffected by convection commonly assumed in most one-dimensional cloud models; 2) the environment characterized by a relatively strong downdraft of saturated or nearly saturated and cooler air. The existence of such saturated downdraft has been known long ago, and their cellular patterns have been revealed more clearly by more recent Doppler radar observations, see, e.g., Ziegler (1978). On the other hand, the downdraft in the far environment is characterized by a much slower sinking motion and a temperature higher than that of the undisturbed state, a consequence of the compressional heating in the stably stratified environment.

The colder and moist downdraft under consideration here is taken as occurring side by side with the updraft and hence its nature is different from the downdraft discussed by Srivastava (1967) and Ogura and Takahashi (1971), where the downdraft is directly created by the falling precipitation in the lower part of the original updraft and hence it represents the decaying stage of the development of the cumulus cloud. One way of creating a downdraft side by side with the updraft is to have the updraft take place along a sloped cold front, such as in the squall line type severe storms. Then the falling precipitation from the updraft can create a downdraft without impeding the updraft. Another way is through the outflow of the raindrop leaden air in the upper layer. Since our simple plume model is not able to describe the details of the development of such downdrafts, here we shall simply assume that such a downdraft is present and try to calculate its influence on the various properties of the system.

3. Numerical procedure

As has been pointed out before, Eq. (18) can be solved directly when the entrainment coefficient μ is taken as known. Therefore the remaining problem is to solve Eq. (21) by making use of the values of θ_v' obtained from (18). Observe that, if q_ℓ is also a known function of z, then (21) can also be integrated directly as a first order equation for y. However, as described in section 4, q_ℓ is a function of w_c. Therefore (21) must be solved together with the liquid water equation. The procedure we adopted in solving these two coupled equations is an

iterative procedure, which is first to solve (21) level by level according to the traditional plume model, that is, by neglecting the pressure perturbation in (21) so that we have $y = w_c^2$, and using $w_c(z_{n-1})$ in the liquid water equation to obtain a first approximation of $q_\ell(z_n)$, and use it in (21) to obtain $y = w_c^2$ for the next level. After the first approximation of w_c is obtained in this way for all levels, we then recalculate w_c from the complete relation (16f) which includes the pressure perturbation, viz.,

$$\frac{R^2}{\alpha^2}\left(w_c \frac{d^2 w_c}{dz^2} - \sigma w_c \frac{dw_c}{dz}\right) - w_c^2 = -y \quad . \tag{21a}$$

This equation is solved by Newton's method as a boundary value problem using the known distribution of y, including possible negative values of y above the y=0 level. Here w_c is required to be positive everywhere except at the top, where it is required to vanish, while at the cloud base w_c is taken as known. Eq. (21) is then solved again for y, using the w_c newly obtained from (21a) to determine a new set of q_ℓ. The procedure is repeated until y and q_ℓ are no longer changing. In most of the calculations presented below we do not include the first order differential term in (21a) which contains the density variation, i.e.,

$$\frac{R^2}{\alpha^2} w_c \frac{d^2 w_c}{dz^2} - w_c^2 = -y \quad . \tag{21b}$$

However as revealed in a later section it is of minor consequence. In all these calculations a grid step equivalent to $\Delta p = 5$ mb is utilized.

The location of the upper boundary for the vertical velocity with pressure perturbation is not known exactly but approximately by the

location of y=0, hence it is used as a first guess with further minor adjustments made during the calculations to give a best fit, i.e., to keep w_c positive and monotonically decreasing near the cloud top. As a final step the upper 15-30 per cent of the vertical velocity profile at the cloud top is checked by recomputing using a marching procedure, making use of existing velocity calculations at lower levels. Typically the only consequence is a slight adjustment in the first or maybe first two non zero values of w_c next to the cloud top while at all other points the solutions normally agree through several decimal places. This small correction is made necessary since the location where w_c=0 is usually not exactly at a grid point but it can be found from the marching solution approximately by interpolating linearly between the last positive and first negative value of w_c.

The presence of a pressure perturbation at the cloud base requires that $d^2w_c/dz^2 \neq 0$ at z=0. An estimate of its value can be obtained utilizing a backward extrapolation technique built around Taylor series expansion and a one sided difference approximation of (21), i.e.,

$$\frac{dy}{dz} + \mu v = g\bar{\beta} \quad , \tag{21*}$$

where y is defined by (21b). Assuming that

$$\frac{1}{M}\frac{dM}{dz} = \mu, \quad M = w_c R^2,$$

the approximation can be shown to be

$$\frac{d^2w_{co}}{dz^2} \approx \frac{(1+2\mu h)\, w_{c1}^2 - (1-\mu h)w_{co}^2 - h\bar{\beta}_o - 2w_{c1}w'_{co}h + h\bar{\beta}_1}{2w_{c1}h^2 + \frac{1}{\alpha}\frac{1}{2}M_1 - M_o(1+\mu h)} \quad . \tag{22}$$

where h = Δz and the subscripts zero and one refer to the variables being evaluated at z=0 and z=h respectively. This expression quickly converges in an iterative process which as a first guess assumes $d^2w_c/dz^2 = 0$ at z=0. Thus the y equation, (21), is solved with an initial value of $y_o = w_c^2$ and then the values of w_c are found from Eq. (21b). This process is repeated allowing for an evaluation of Eq. (22) which gives a correction for the initial value of y_o until the change in y at z=0 is less than .002 m^2s^{-2}. Then the procedure is as described above. As a general rule, with some minor exceptions, it is found that clouds of small radii, say < 1000 m, have final values of y_o slightly larger than w_{co}^2 whereas larger radii clouds have final values less than w_{co}^2. In our model the overall consequence of these changes in y_o, of order unity or less, is very small but included for completion.

Other important quantities utilized in our calculations are the following:

entrainment coefficient, $\mu = .183/R$;

latent heat of condensation, $L = 597.0 - .555(T-273K)$ CAL gm^{-1};

gravity, $g = 9.814\ ms^{-2}$;

virtual temperature, $T_v = (1 + .608q)T$;

and finally we used $\alpha''=0$, i.e., zero viscous diffusion.

4. The calculation of liquid water.

Liquid water exerts a negative buoyancy upon the updraft, as evident in the effective buoyancy term, Eq. (21), so its concentration must be computed simultaneously with the vertical velocity. Liquid water, $q_{\ell w}$, is really the sum of cloud and rain water where cloud water, denoted by $q_{\ell c}$, is composed of small droplets that are carried by the updraft and rain water, denoted by $q_{\ell r}$, is composed of the larger drops that fall relative to the updraft. Condensation loads the cloud via cloud water whereas precipitation, i.e., the fallout of rainwater, unloads the updraft. This unloading is important lest the drag force becomes too unrealistic. A detailed relationship between q_{cw} and q_{rw} has been outlined by Kessler (1969). Here a simpler format, similar to that used by Anthes (1977) based on a median dropsize is followed.

Cloud water is known to increase due to the condensation process and to decrease because of the autoconversion process which creates raindrops and by collection of cloud droplets by raindrops. Thus in symbolic form,

$$\Delta q_{cw} = \Delta q_{cond} - (\Delta q_{cw})_{auto} - (\Delta q_{cw})_{coll} . \tag{23}$$

The autoconversion process, following Kessler (1965), is given by

$$(q_{cw})_{auto} = \begin{cases} K\Delta t(q_{cw}-a') & q_{cw} \geq a' \\ 0 & q_{cw} < a' \end{cases} , \tag{24}$$

where $a' = 0.5$ gm m^{-3} is the threshold value and $K = 10^{-3}s^{-1}$. The collection term is expressed as

$$(\Delta q_{cw})_{coll} = 5.26 \times 10^{-3} q_{cw} q_{rw}^{0.875} \Delta t . \tag{25}$$

Rainwater increases at the expense of cloud water and decreases due

to fallout, thus symbolically,

$$\Delta q_{rw} = (\Delta q_{cw})_{auto} + (\Delta q_{cw})_{coll} - (\Delta q_{rw})_{fallout} \quad . \tag{26}$$

It will be assumed that the fallout rate is proportional to both q_{rw} and the terminal velocity V_F, so that we have

$$(\Delta q_{rw})_{Fallout} = \lambda q_{rw} V_F \Delta t, \tag{27}$$

where λ is an empirical fallout coefficient whose dimension is 1/length and hence it is often written as 1/H (Anthes 1977, Krietzberg and Perkey, 1976). Here both q_{cw} and q_{rw} are expressed in gm m^{-3} and the time step Δt is computed from $\Delta z/w_c$ for $w_c \geq 0.005$ ms^{-1}.

Following Simpson and Wiggert (1969), we take V_F for the median size rain drops as given by the following formula in terms of q_{rw}

$$V_F = 5.1\ q_{rw}^{0.125}\ ms^{-1} \quad . \tag{28}$$

The rate of precipitation, P_R(gm $s^{-1}m^{-2}$) per square meter can be computed using

$$P_R = \sum_{i=1}^{N} \Delta t_i\ V_F(\Delta q_{rw})_{Fallout}/t \quad , \tag{29}$$

where Δt_i is the time since development of the i^{th} layer of thickness Δp and

$$t = \sum_{i=1}^{N} \Delta t_i$$

is the total cloud development time. It is customary with plume models to equate total cloud lifetime and development time.

5. Discussion of Results.

In this study the characteristic properties of cumulus convection are investigated by the use of a simple quasi-Lagrangian axi-symmetric steady state model based on the two-dimensional vorticity and heat equations which include the effects of both the pressure perturbation and the influence of downdrafts in the environment. These equations are reduced to one-dimensional forms by integrating them from the center of the plume outward into the environment. The entrainment terms of Stommel (1947) in which the interaction between the cloud and environment is represented by an expression inversely proportional to the cloud radius are recovered in this manner. In our formulation additional terms are introduced when nearby environmental temperature and relative humidity profiles differ from the undisturbed state far removed from the cloud. These relatively nearby environmental variations owe their existence to the updraft and their inclusion into the model's physics is distinctly different from the lateral mixing utilized by Ogura and Takahashi (1971). The influence of the compensating nearby downdrafts, transports of heat and mass, upon the total cumulus convection has been shown to be of major importance in several observational studies (Johnson, 1976; Nitta, 1978; Zipser, 1977, others). According to Nitta (1978), during the active stage of the deep cloud clusters strong downdrafts exist with vertical velocities (amplitudes) about 40-50% of the adjacent updrafts.

Two different undisturbed environmental situations are investigated by our model, namely, 1) a potentially more unstable environment represented by mean Gulf of Mexico hurricane season temperature and relative

humidity profiles (Herbert and Jordan, 1959) and 2), for later consideration, a less unstable sounding in the middle latitude. Fig. 1 illustrates the potential (solid line) and equivalent potential temperature (dashed and dotted curves) of the mean tropical sounding. Two θ_{oE} curves are given in this figure, the very small differences between them are due to the fact that, in the dashed curve the latent heat of vaporization is taken as constant, namely, L = 600 cal gm^{-1}, whereas in the dotted curve L = 597 - .555t is used, where t is in ^{o}C, and the latent heat of freezing, 80 cal gm^{-1}, is also included linearly between -10 and $-40^{o}C$. Fig. 2 shows the vertical derivative of the entropy S_{os} for the constant L case, which appears as a forcing function in the perturbation entropy Eq. (19). A positive contribution by this term is indicated below 595 mbs. Unless stated otherwise all figures refer to calculations using this mean tropical sounding.

Here we shall present the results based on (21b) first, that is, with $\sigma = 0$. The cloud temperature excesses obtained from our plume model for a cloud with R = 1000 m are illustrated in Fig. 3. Here the dashed curve is with moist downdraft while the solid curve is without moist downdraft. The relative humidity of the downdraft is taken as 95 per cent. It is seen that the downdraft air is cooler than the undisturbed air represented by the mean sounding and as a consequence the overall depth of the cloud is reduced by nearly 60 mb in pressure measure. As shown in Fig. 4, the corresponding reduction of the vertical velocity is substantial. Both of these changes are the results of the reduction of the buoyancy, which itself is directly attributable to the fact that, even though the moist downdraft temperature T_{dw} is lower than the temperature T_{o} of the undisturbed environment, the virtual temperature

perturbation ($T_{V_{dw}} - T_{V_o}$) is positive on account of the higher mixing ratio of the moist downdraft. This tendency can be reversed if T_{dw} becomes much lower than T_o. Our calculations show that, for the same temperature and humidity distributions, the influence of the downdraft on the buoyancy decreases with increasing cloud radius and vice-versa. These results are not significantly affected by the presence of other physical processes such as evaporation at the cloud boundary or inclusion of latent heat of fusion, as illustrated by the dotted curve in Fig. 2 and dashed curve in Fig. 5, respectively. The latter effect is introduced by incorporating the latent heat of freezing linearly between 0 and $-10^{o}C$.

The consequences of environmental compressional heating upon cloud potential temperature excesses when no nearby moist downdraft is present are displayed in Fig. 6 for three cloud radii. The solid lines represent the cloud perturbation in the absence of compressional heating. The overall effect, as revealed in the dashed curves (with a=0.4), is to warm the updraft especially at upper levels. The vertical velocity however is reduced because of the net reduction in buoyancy due to the term -a/2 in Eq. (21) that more than compensates for the enhanced cloud temperature excesses. This is clearly seen in Fig. 7 by comparing the profiles computed with (dotted curve) and without (dashed curve) compressional heating.

For a small radius cloud, R = 500 m (Fig. 7), the large changes in the vertical velocity due to compressional heating dwarfs the influence due to pressure perturbation. The latter causes a very minute reduction as indicated in Fig. 7 by the differences between the solid (no pressure perturbation) and dashed curves. However, increasing the cloud radius to

5000 m substantially enhances the role of the pressure perturbation so that these two influences become nearly equivalent in importance. The effect of the pressure perturbation as revealed in this figure and in others, shown and not shown, is to reduce the magnitude of the vertical velocity, to shift the maximum vertical velocity, w_{max}, downward and to slightly increase the cloud's depth, as can be seen from a comparison between the solid and dashed or dashed-dot curves in Fig. 8, while the dotted curve illustrates the influences of compressional heating in the environment. The distinction between the dashed and dashed-dot curves, both of which contain pressure perturbation, is that in the latter the σ term in Eq. (21a) is included. The influence of this term is to further reduce the velocity by a small amount except near the cloud top where w_c is enhanced by it. The value of w_{max} is only slightly decreased but shifted upward in this deeper cloud. The general trend with or without the inclusion of this first order term is much the same hence this term is ignored in most of our calculations. These conclusions about the pressure perturbation are in major agreement with those of Yau (1979) obtained using analytical models.

Holton (1974) has found by the use of an one-dimensional Eulerian cloud model that for clouds with radii greater than 1 km, the pressure perturbation substantially reduces the growth rate. Within the framework of our Lagrangian model it is not possible to compute the growth rate. On the other hand, another very interesting effect of the pressure perturbation is revealed by our solutions, namely, when the pressure perturbation is included, w_{max} achieves its highest value when the cloud radius is

about 8 km, whereas in the absence of the pressure perturbation w_{max} increases monotonically with increasing radius, as can be seen from the solid and the dashed curves in Fig. 9. Our results also show that small clouds are only slightly effected by the pressure perturbation but, as already known previously, are greatly influenced by the entrainment effect which is inversely proportional to the radius, whereas for large cloud the reverse is true. Thus the presence of the optimal cloud size when both of these two factors are taken into consideration appears to represent a balance between these two opposing effects.

The importance of the initial updraft radius and velocity is shown in Fig. 10 for three vertical velocity profiles computed using a constant mass flux, $M_c = w_c R^2$, at the cloud base. The three profiles differ considerably at higher levels due mainly to the entrainment processes, thus indicating especially the importance of the proper choice of the updraft radius. Squire and Turner (1962) in contrast did not obtain this large variation mainly due to their use of the theoretical saturated environmental sounding. For radii much larger than those considered here, e.g., R = 10,000 m, the importance of entrainment is replaced by the importance of the pressure perturbation, and in contrast to the results in Fig. 10, the largest radius cloud will have the smallest vertical velocity maximum. Nevertheless, the largest cloud will have the deepest penetration.

Many previous investigations have attempted to account for the influence of the pressure perturbation by utilizing a reduced gravity, i.e., in the vertical velocity equation g is replaced by $g/(1+F)$, where F

is usually assigned a constant value of about 0.5 and the pressure perturbation term is otherwise neglected completely. As previously pointed out the pressure perturbation is included in this model since the vertical variation of ϕ is retained in the vorticity equation. But if in Eqs (21b, 21a) we define

$$\beta = \frac{-R^2}{\alpha^2 w}\frac{d^2 w}{dz^2},$$

then for the special case β equals a constant the modified gravity formulation is obtained. In reality β is not constant as shown in Fig. 11. For this mean tropical sounding note that the reduction of the effective buoyancy is generally much less than the commonly used factor 2/3. Fig. 12 shows another set of β profiles from an individual Salem III. sounding which contains several stable layers above the cloud base at 83.64 mb_2, as indicated by positive values of $\partial S_{os}/\partial z$ in Fig. 13. The β profiles for R = 2000 and 5000 m represented by the dashed and solid lines in Fig. 12, respectively, exhibit large variations and a region of negative values, indicating that the pressure perturbation force acts to partially counteract the buoyancy, thus smoothing out the vertical velocity profiles as shown in Fig. 14. A cloud of small radius, R = 1000 m, is unable to break through the stable layers whereas the 2000 and 5000 m radius clouds are capable but their vertical velocity profiles are still influenced by it. With the pressure perturbation, as represented by the dashed curves, the impact of the stable layers are substantially reduced, especially for the 5000 m radius or still larger clouds.

The perturbation pressure inherit in our solutions can be solved for

directly by integrating the traditional vertical velocity equation using our computed velocities. The vertical profiles of the scaled perturbation pressure, $\pi^* = \pi - \pi_o$, where π is the ratio of the perturbation pressure divided by environmental density, is found to be negative at low levels and positive near the top of the cloud as shown in Fig. 15 for cloud radii of 2000 (dotted curve), 5000 (dashed curve) and 10,000 m (solid line). The unknown constant of integration π_o was assigned the value of π at 400 mbs. The slope of each curve, i.e., $\partial\pi^*/\partial z$, indicates the degree to which the buoyancy is adjusted by the non-hydrostatic pressure perturbation. Positive slope implies that the buoyancy is reduced whereas negative slope indicates an enhanced buoyancy, as found, for example, near the cloud top. The Salem Ill., π^* profile, not shown, contains a negative slope between 667.64 and 472.64 mbs, showing that the pressure perturbation, in part, is offsetting the reduction in buoyancy caused by the stable layers found in the sounding between 732 and 572 mbs.

In Fig. 16 the perturbation pressure profile is displayed in the same format as π^* above. Note the exceedingly small values of less than 0.2 mbs for R = 2000 m (dotted line) and the large positive and negative values at the cloud base and top, respectively, for a radius of 10,000 m (solid line). Also, with compressional heating (dashed-dot curve), there is a slight reduction when compared against the no compressional heating case, as represented by the dashed curve.

Vertical profiles of the average liquid water concentration for cloud radii of 500 (dotted curve), 2000 (dashed curve) and 5000 m (solid line), after fallout, are shown in Fig. 17. It is seen that associated

with increasing cloud size, and hence larger vertical velocities, is the upward movement of the maximum $q_{\ell w}$ toward the cloud top. A similar trend is not clearly evident in the fallout rate within each 5 mb interval as illustrated in Fig. 18 for the same cloud radii. Except for the 500 m cloud (dotted curve) the fallout rate is a maximum at nearly the middle point of the vertical profile. The total precipitation rate, for the tropical sounding without ice phase, is 1.57, 4.73 and 5.17 cm hr^{-1} for cloud radii of 500, 2000, and 5000 m respectively. The addition of the ice phase will increase the precipitation rate to various degrees, roughly 10-25 per cent depending on details of its inclusion. In these calculations the constant of proportionally λ in the fallout term, Eq. (27), is equated with R^{-1} for 100 m $\leq R \leq$ 2000 m and $\lambda = 5 \times 10^{-4} m^{-1}$ for $R >$ 2000 m. The Salem Ill. sounding, with an ice phase inserted linearly between -10 and -40°C and with $\lambda \geq 6.6 \times 10^{-4} m^{-1}$, produces precipitation rates of 0.69, 5.34 and 5.79 cm hr^{-1} for cloud radii of 1000, 2000 and 5000 m respectively. The large increase between 1000 and 2000 m is due to the fact that for the larger radius the cloud is able to penetrate the stable layers and reach a considerable height.

It should be pointed out that the precipitation rates given above represent the average precipitation rates for the developing period of the different types of clouds only. If, instead of decaying, the deep cumulus cloud and its circulation remain in a semi-steady state after fully developed, then the precipitation rate can be much higher than the values given above since then almost all the water vapor coming into the cloud through its base and sides will be precipitated.

6. Influence of cumulus convection on the mean properties of the atmosphere.

We have illustrated how environmental factors near the updraft can influence the basic cloud properties. The reverse process, i.e., the net effect of short lived cumulus convection upon the thermodynamic, moisture and momentum structure of meso and synoptic scale systems has been recognized for years. Various parameterization techniques have been introduced to incorporate the vertical distributions of condensation heating and momentum transfer into the large scale flow, see, e.g., Kuo (1965, 1974), Kreitzberg and Perkey (1976) and Anthes (1977).

It is well known that the overall effect of cumulus convection is to warm its surroundings. The contribution to the mean heating from a single cloud is from the combination of the latent heat and the upward transport of sensible heat. We want to compute the mean heating rate, $\partial T/\partial t$, produced by the cumulus convection, including both the effects of the compressional heating in the far environment and the effect of the moist and cool downdraft. Let us represent the areas of the updraft, moist downdraft and far away downdraft by A_c, A_{dw} and A_d, respectively, and let the vertical velocities in these areas be w_c, w_{dw}, and w_d. Then the condition of zero net vertical mass flux can be taken as

$$A_c w_c + A_{dw} w_{dw} + A_d w_d = 0, \tag{30}$$

where the influence of the difference in density in the different areas has been disregarded for simplicity. Further, we shall express w_{dw}, σ'_{dw} and A_{dw} in terms of w_c, σ'_c and A_c of the cloud updraft by introducing the non-negative factors of proportionality α_2, γ and k and writing them as

$$w_{dw} = -\alpha_2 w_c, \quad \theta'_{dv} = a\theta'_c, \quad A_{dw} = kA_c. \tag{31a,b,c}$$

On substituting these relations in (30) we then obtain

$$A_d w_d = -(1 - \alpha_2 k) A_c w_c. \tag{32}$$

We consider that the heating effect of the cumulus convection in the layer Δz is produced by the following three different processes:

i) the net upward transport of sensible heat into this layer inside the cloud and in the convective moist downdraft in the immediate environment;

ii) the compressional heating created by the slow descending motion in the far away environment;

iii) the release of latent heat in the cloud updraft.

Here the first two processes are directly concerned with the sensible heat while iii) is due to the latent heat. We shall calculate these three contributions separately below.

According to the relations (31a,b,c) the area average of the upward heat transport T^*_θ inside the cloud and its immediate moist environment is given by

$$T^*_\theta = (1 - \alpha_2 ak) a_o w_c \theta'_c, \tag{33}$$

where

$$a_o = \frac{A_c}{A}. \tag{33a}$$

Thus, on using R^2 to represent A_c for the axisymmetric cloud we find that the mean heating effect produced by the first process is given by

$$\frac{\partial T}{\partial t}_{1,1} = -\frac{1}{\pi_o \rho} \frac{\partial}{\partial z}(\rho T^*_\theta). \tag{34}$$

The contribution of the compressional heating in the far environment to the mean heating can be taken as given by

$$\frac{\partial T}{\partial t}_{1,2} = -\frac{A_d w_d}{A \pi_o} \frac{\partial \theta_o}{\partial z} \frac{A\hat{t}}{\hat{t}},$$

where $\Delta t/\hat{t}$ is the ratio of the existence of the cloud at the level z to the total time $\hat{t}$ of existence of the cloud. Thus, on making use of the relation (32) we then find

$$\frac{\partial T_{1,2}}{\partial t} = (1 - \alpha_2 k)\frac{a_o w_c}{\pi_o}\frac{\Delta\hat{t}}{\hat{t}}\frac{\partial \theta_o}{\partial z} . \tag{35}$$

The sum of these two effects represents the total heating from sensible heat. We shall represent this sum by $\partial T_1/\partial t$, viz.,

$$\frac{\partial T_1}{\partial t} = -\frac{1}{\rho\pi_o}\frac{\partial}{\partial z}(\rho T_\theta^*) + (1 - \alpha_2 k)\frac{a_o w_c}{\pi_o}\frac{\Delta\hat{t}}{\hat{t}}\frac{\partial \theta_o}{\partial z} \tag{36}$$

where T_θ^* is given by (33).

The heating due to the release of latent heat can be taken as

$$\frac{\partial T_2}{\partial t} = -a_o \frac{L}{c_p} w_c\left[\frac{\partial q_s}{\partial z} - \mu(q^* - q_s)\right] , \tag{37}$$

where q^* is the value of q just outside the updraft. From the results given above we find that the total heating rate is given by

$$\frac{\partial T}{\partial t} = \frac{\partial T_1}{\partial t} + \frac{\partial T_2}{\partial t} , \tag{38}$$

where $\partial T_1/\partial t$ is defined in (36) and $\partial T_2/\partial t$ in (37).

Note the reduction in the heating rate profile shown in Fig. 19 for a 1000 m updraft, computed with the effect of a moist and cool downdraft (dashed line) as opposed to that computed without this effect (solid line). Here the ratio of moist downdraft area to the updraft area, i.e., $k = A_{dw}/A_c$, is taken as 1.0, and the ratio of vertical velocities, $\alpha_2 = -w_{dw}/w_c$, is taken as 0.4. In both cases the role of compressional heating has been included, assumming that the ratio of updraft area to total area, i.e., $A_c/A = a_o$ is 0.1. The total sensible heating profile for the moist downdraft case (dashed-dot curve), is slightly negative at

low levels and only slightly positive at high levels. Thus latent processes are responsible for most of the total heating. The contribution of the compressional heating in the environment to the total sensible heat is indicated by the dotted curve.

The significance of latent heating (dotted curve) is shown in Fig. 20 for a 2000 m radius cloud containing compressional heating, along with the total sensible heating rate (dashed curve) and their sum, i.e., the total heating rate (solid line). Note the importance of the total sensible heat contribution near the cloud top but otherwise the heating is due mainly to latent heat. This peaking near the cloud top is even more pronounced in the 'cloud' sensible heating rate (dashed-dot curve, Fig. 21) for a 5000 m radius cloud. The magnitude of the negative contribution at lower levels is also fairly large but is considerably diminished provided the positive contribution from compressional heating (dotted curve) is added to form the total sensible heating rate. The importance of compressional heating is revealed also in Fig. 21 by the difference between the total heating rate computed with environmental effects, $a = 0.4$, $b = -c_p/L\pi$, (dashed curve) as compared with the 'cloud' total heating rate (solid line). Note that this difference is smaller in magnitude than the contribution from compressional heating itself (dotted line). The reason why is because compressional heating also reduces the vertical velocity, thereby reducing the local rate of latent heat released. This effect is illustrated further in Fig. 22 for three different cloud radii. Some measure of the increase of the total heating rate with increasing cloud radius can also be gained by comparisons between the solid

curves in Figs. 19 and 20 and the dashed curve in Fig. 21. For clouds of radius R = 1000 m the total heating rate maximum is located nearly midway in the vertical profile, but it is shifted upward toward the cloud top as the radius is increased.

We have shown that for large cloud radii, e.g., R = 5000 m, compressional heating increases the total heating rate. This conclusion is also valid for cloud radii of 2000 and 500 m (not shown), but obviously proportionally less. For the range of parameters considered, the role of the moist and cool downdraft is found to increase the sensible heat transport T_θ^* (Eq. 33) slightly by the addition of the small positive factor $(-a_2 ak)$ in T_θ^* but also shown to reduce the vertical velocity, so that there is some net reduction in the total heating rate by this effect.

It should be pointed out that the expression (37) for the heating rate from latent heat is based on the total condensation rate. When the cloud dissipates, the liquid water carried by the cloud will re-evaporate and therefore the mean net heating rate produced by the cloud during its whole life span should be given by

$$\frac{\partial T}{\partial t} = \frac{\partial T_1}{\partial t} + \frac{\partial T_2}{\partial t} - \frac{A_c L q_{\ell w}^{(e)}}{A \pi_o \bar{\rho} c_p}, \tag{39}$$

where $q_{\ell w}^{(e)}$ stands for the amount of liquid water re-evaporated into the environment. The rate of moistening of the atmosphere is given by

$$\frac{\partial q_o}{\partial t} = \frac{A_c}{A} (q_s - q_o + q_{\ell w}^{(e)}). \tag{40}$$

Because of our lack of more reliable knowledge of the relation between the cloud type and $q_{\ell w}^{(e)}$, the influence in re-evaporation of the cloud

water into the environment has not been included in our calculations yet. If we assume that all the unprecipitated liquid water drops in the cloud are re-evaporated into the environment at the same level as they occur in the cloud as the cloud dissipates, then a larger cooling will take place near the cloud top than at low levels as the cloud dissipates.

It is evident that the various area mean effects produced by a specific type of cumulus can be calculated by the use of the cloud model provided the area ratio a_0 ($=A_c/A$) and the other physical parameters are known. Obviously, a model cloud representative of the average conditions can also be constructed by combining a number of clouds of different radii. The heating and transporting influences of such a cloud can be obtained from those of the individual clouds by assigning proper weighting factors to them.

The use of the mean stability and boundary layer properties of the atmosphere and large- and meso-scale lifting to determine whether cumulus convection will occur or not in the region, and to use the large- and meso-scale net convergence of moisture as the measure of the average condensation rate in such systems as proposed by the first author (Kuo, 1961, 1974) still appear to be the proper road for the paramatic representation of the time and space average heating effect of cumulus convection. However, the question of whether cumulus convection will occur at a given locality and a given time can not be answered by utilizing large scale properties alone. The problem is complicated further by the fact that, cumulus convection is of the nature of overturning and hence, if restricted to a small region, it can occur only once and after completing this process the stratification will become stable and the moisture content exhausted. On the other hand, if the convection takes an organized form with a continuous supply of

moist air from far away, such as those in the meso-scale storms, then the system can have a much longer life. Evidently whether such a system will be created in a given region or not can only be determined by studying the general dynamic and thermodynamic conditions, and not by using the mean large scale stratification and transport properties alone.

In view of the many uncertainties concerning the average heating effect of cumulus convection, it appears preferable to determine it by a less involved simple method rather than by the use of a detailed model. One simple way is to use the vertical distribution of the potential temperature excess θ_c' given by (18) or T_c' given by (18b) as the vertical distribution of the heating rate. On comparing the total heating profiles in Figures 19, 20, and 21 for clouds with radius greater than 1000 m with the cloud potential temperature profile in Fig. 6 we see that they are fairly similar to each other, indicating that the distribution of the potential temperature excess θ_c' can be used as a reasonable approximation to the vertical distribution of the mean heating effect created by the cloud activity, as proposed by [illegible] ([illegible]).

The question of how the latent heat and sensible heat accumulated in an individual cloud is transmitted to the mean atmosphere may also be discussed. Here at least two different processes can be visualized, namely, a) by random and equal chance distribution of the cloud population in time and space over a large area and longer time span and b) by excitation of large scale circulation and dispersion. Both of these two processes are effective in the atmosphere and such effects can be taken as have been included in the parameterization scheme.

Finally, the effect of cumulus convection on the horizontal velocity [illegible]

$$\left(\frac{\partial \bar{V}}{\partial t}\right)_{cu} = -\frac{A_c}{\rho A}\frac{\partial}{\partial z}\left[\rho w_c (V - V_b)\right] . \qquad (41)$$

7. Summary.

A quasi-one-dimensional and quasi-Lagrangian steady state model which takes into consideration the influences of the pressure perturbation, vertical density stratification and nearby moist downdraft on the axisymmetric cumulus cloud convection is obtained by integrating the combined heat and moisture equations and the azimuthal vorticity equation from the cloud center to the outer edge and utilizing various entrainment considerations. This model shows that the influence of the pressure perturbation is proportional to the square of the cloud radius and hence it is small for small clouds. This model is used to investigate the variations of the various cloud properties with the radius of cloud under two different environmental conditions, one is for the potentially more unstable and more smooth mean tropical atmosphere during the hurricane season while the second is for a less unstable middle latitude environment with prominent thin stable layers in mid-lower troposphere. Further, two different kinds of cumulus convection are considered, namely, A) is of the form of a simple updraft surrounded by the almost unaltered far environment, either with or without a feed back from the compressional heating in this environment, while B) is with a nearly saturated and cooler nearby downdraft, as is often observed in the cloud clusters in the tropics. In this latter case the cloud is not influenced by the far environment directly.

It is found that the pressure perturbation in the cloud can reach from $\pm$ 2.5 to $\pm$ 7 mb at the cloud base and the cloud top as the radius of the cloud increases from 5 km to 10 km but is small for cloud radius

less than 2 km. Further, the magnitude of the perturbation pressure is reduced by the inclusion of the temperature feed back from the compressionally heated environment.

Since the temperature equation (18) involves neither the pressure nor the vertical velocity, the pressure perturbation has no direct influence on the cloud temperature excess. On the other hand, the inclusion of the pressure perturbation reduces the vertical velocity in the cloud, as it must since pressure perturbation transmits energy to the environment. One interesting and possibly also important effect of the pressure perturbation is that it gives rise to an optimal cloud radius of about 8 km, corresponding to the highest value of w_{max}, under the tropical environment, while without the pressure effect w_{max} increases monotonically with increasing R.

The influence of the density stratification is to reduce w_c slightly below the level of w_{max} and to increase w_c above this level and also to increase the cloud depth slightly, but the total influence is not prominent. The results show that, for the normal tropical atmosphere, the cloud properties change gradually with the cloud radius, while for the less unstable environment with prominent stable layers in mid-lower stratosphere, the cloud properties change abruptly as the cloud radius increases from less than to larger than 2 km, reflecting the inhibiting influence of the shallow stable layer in mid-lower troposphere on the smaller clouds.

It is also found that the presence of a moist but cooler convective [illegible] reduces both the updraft and the cloud depth. It also

augments the precipitation rate, especially for the smaller clouds.

The heating and moistening influences of cumulus cloud convection on the large scale atmosphere have also been calculated by the model. It was found that the main part of the heating is from the latent heat but compressional heating of the environmental air is also of importance, especially close to the top of the cloud. On comparing the average heating rate with the potential temperature excess θ_c' given by this model we find a close similarity between them for cloud radius larger than 1 km. It is therefore concluded that θ_c' can be used as a rough approximation to the vertical distribution of the average net heating effect produced by cumulus convection in the parameterization scheme. Of course, results obtained from detailed calculations from the cloud model can also be used.

An equation for the vertical mixing of the horizontal momentum by cumulus convection on the change of the horizontal velocity has also been obtained.

Acknowledgement

This work is supported by the Air Force Geophysics Laboratory through Contract AF F-19628-77-C-0044.

Appendix: List of Symbols

(r,z) radial distance from the axis and altitude

u,w radial and vertical components of velocity

w_c mean vertical velocity of cloud updraft

p_o, ρ_o, T_o, θ_o, q_o: pressure, density, absolute temperature, potential temperature and water vapor mixing ratio in the undisturbed environment, all taken as functions of the altitude z only

p', T', θ' $(= \pi T')$, q': mean values of departures of the total pressure p, temperature T, potential temperature θ and water vapor mixing ratio q in the cloud from the undisturbed values p_o, T_o, θ_o and q_o.

$T_v = T(1 + 0.609q)$: virtual temperature of moist air

$\theta_v = \pi T_v$ virtual potential temperature

C_p specific heat at constant pressure

R 1) gas constant of dry air; 2) radius of cloud updraft

$(\frac{1000\ mb}{p})^{R/c_p} = \pi_o$

$q_s(T)$, q_{os} saturation mixing ratio at temperature T of cloud and at temperature T_o of environment

$q'' = q_s(T) - q_{os}$

$q_w = q_{cw} + q_{rw}$ liquid water mixing ratio in cloud updraft; q_{cw} is cloud liquid water mixing ratio and q_{rw} is mixing ratio of rain water in gm m^{-3}

C rate of condensation

L latent heat of condensation, which may also include the latent heat of freezing

$\bar{\theta}$ constant average value of θ_e

$\theta_e = \theta + Lq/c_p$ equivalent potential temperature

$\theta_{oe} = \theta_o + Lq_o$, $\theta_{oes} = \theta_o + Lq_{os}/c_p$

s, s_o, $s_{os} = (\theta_e, \theta_{oe}, \theta_{oes})/\bar{\theta}$

$s' = s - s_o$, $s'_c = s_{cloud} - s_{os}$;

σ density stratification factor $= -\partial \log \rho/\partial z$

$a = \theta'(R)/\theta'$; $b = q'(R)/q'$; $a' = s'(R)/s'_c = a(c_p \bar{\theta} + bL\epsilon)/(c_p \bar{\theta} + L \partial q_s/\partial T)_c$

$\alpha_1 = U(R)/w$; $\beta_1 = \eta(R)/\eta$; $\alpha'_1 = \alpha_1 \beta_1$

$\alpha^* = 2\alpha_1 a'$; a_2 = coefficient of evaporation effect at $r = R$

μ mass entrainment coefficient $= 2\alpha_1/R$

α'' coefficient of eddy diffusion effect

ψ stream function for u and w

$\alpha(= 2.405)$ radial variation coefficient of ψ

e_s saturation vapor pressure

a' threshold value of cloud liquid water q_{cw}

K coefficient of cloud drop autoconversion process

V_F average terminal velocity of rain drops

P_R precipitation rate

$\lambda = 1/H$ empirical fallout coefficient

q_ℓ liquid water mixing ratio, in gm per gm

k area ratio of moist downdraft to updraft

a_2 ratio of moist downdraft velocity to updraft velocity

List of Figures

Fig. 8. Same as Fig. 7 except for a 5000 m radius cloud. Dash-dotted curve is without compressional heating but with both the σ term in (21a) and pressure effect included and is to be compared with dashed curve.

Fig. 9. Variation of w_{max} with cloud radius with (dashed curve) and without (solid line) pressure perturbation.

Fig. 10. Vertical velocity profiles for 3 different cloud radii taking the cloud base mass flux as constant. 1) $w_o = 2\ ms^{-1}$ and $R = 2000\ (2)^{-1/2}m$ (dotted curve); 2) $w_o = 1\ ms^{-1}$ and $R = 2000$ m (solid line); 3) $w_o = 0.5\ ms^{-1}$ and $R = 2000 \times 2^{1/2}m$ (dashed curve).

Fig. 11. Vertical profiles of gravity reduction factor β for R = 500 m (dotted curve), R = 2000 m (dashed curve) and R = 5000 m (solid line).

Fig. 12. Same as Fig. 11 except for Salem Ill. sounding in Fig. 13.

Fig. 13. Vertical profile of $\partial \hat{S}_{os}/\partial z$ for a 1800 C.S.T. Salem Ill. sounding (8/22/75).

Fig. 14. Vertical velocity profiles for 3 radii obtained with the Salem, Ill. sounding. Dashed curves include pressure perturbation, solid lines: without pressure effect.

Fig. 15. Variation of perturbation pressure to density ratio π^* with height in cloud for mean hurricane season sounding for cloud radii R = 2000 (dotted curve), R = 5000 (dashed curve) and R = 10,000 m (solid line). No compressional heating.

Fig. 16. Profiles of the perturbation pressure plotted in the same format as π^* in Fig. 15, with the addition of the dashed-dot curve computed including compressional heating for a 5000 m cloud.

Fig. 17. Vertical profiles of the liquid water concentration, $q_{\ell w}$, for cloud radii of 500 (dotted), 2000 (dashed) and 5000 m (solid curve).

Fig. 18. Same as Fig. 17 except showing the fallout rate within each 5 mb interval.

Fig. 19. Heating rates for cloud of radius 1000 m, $a_o = 0.1$, $k = 1.0$, and $a_2 = 0.4$, computed with ($a = -0.1$, $b=0.002$, dashed curve) and without ($a = 0$, solid) moist downdraft. The total sensible heating profile is indicated by the dashed-dot curve and the contribution of compressional heating by the dotted curve.

Fig. 20. Vertical profiles of the total sensible heating rate (dashed curve), the latent heating rate (dotted curve) and their sum (solid line) for a 2000 m cloud with compressional heating ($a = 0.4$, $b=-\frac{c_p}{L\pi}$)

Fig. 21. Heating rate of a 5000 m cloud. Dashed curve: total heating rate with compressional heating in environment and $a=0.4$, $b=-c_p/L\pi$; solid curve: total heating rate produced by cloud alone; Dash-dotted curve: 'cloud' sensible heating under influence of compressional heating in environment; Dotted curve: contribution from compressional heating in environment alone.

Fig. 22. π_o times the local rate of latent heating for 3 different cloud radii with ($a = 0.4$, $b = -c_p/L\pi$ dashed curve) and without ($a = 0.0$ solid line) compressional heating, without moist downdraft.

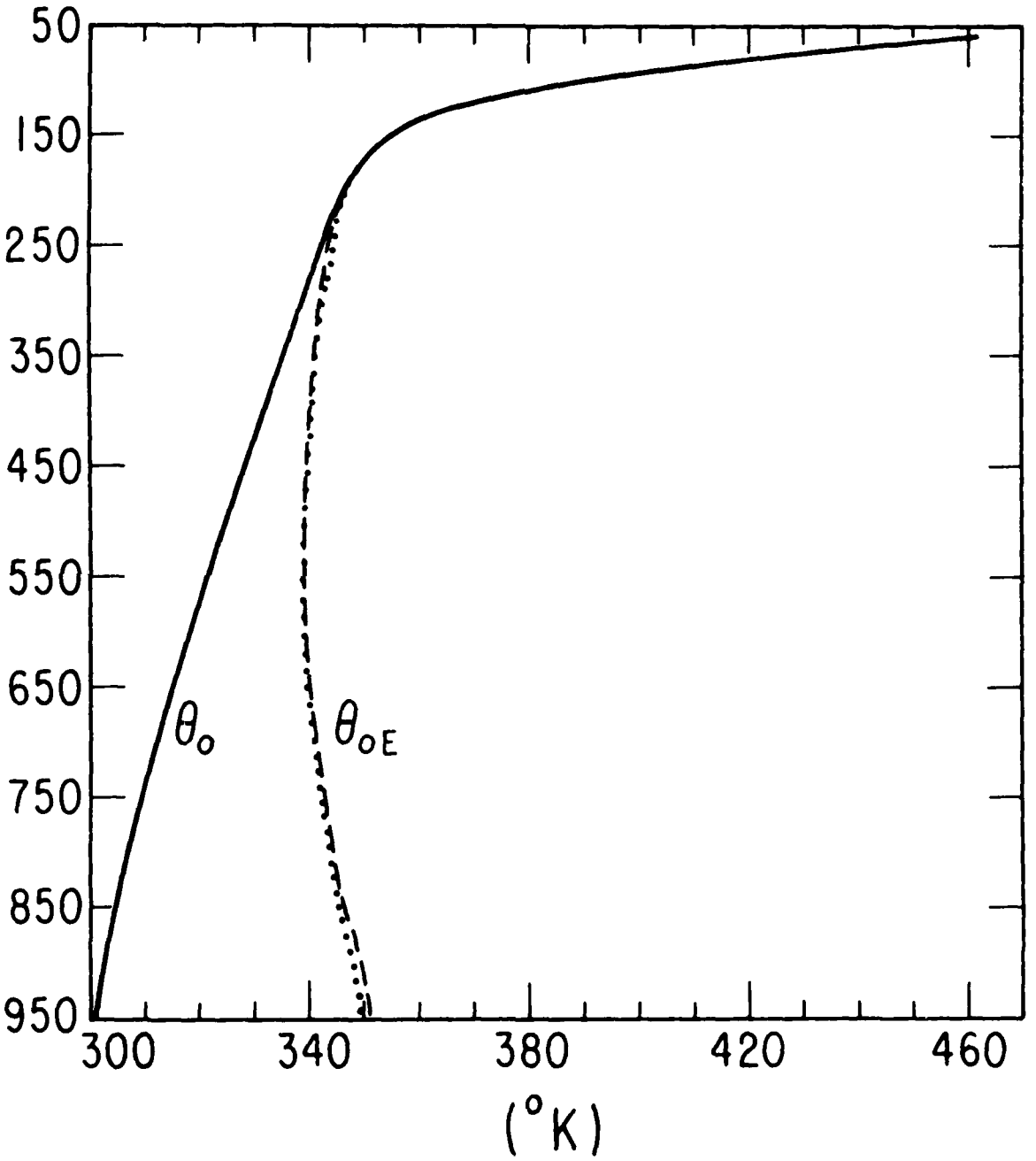
50
150
250
350
450
550
650
750
850
950
300
340
380
420
460
(°K)
θ_o
θ_{oE}

Fig. 1.

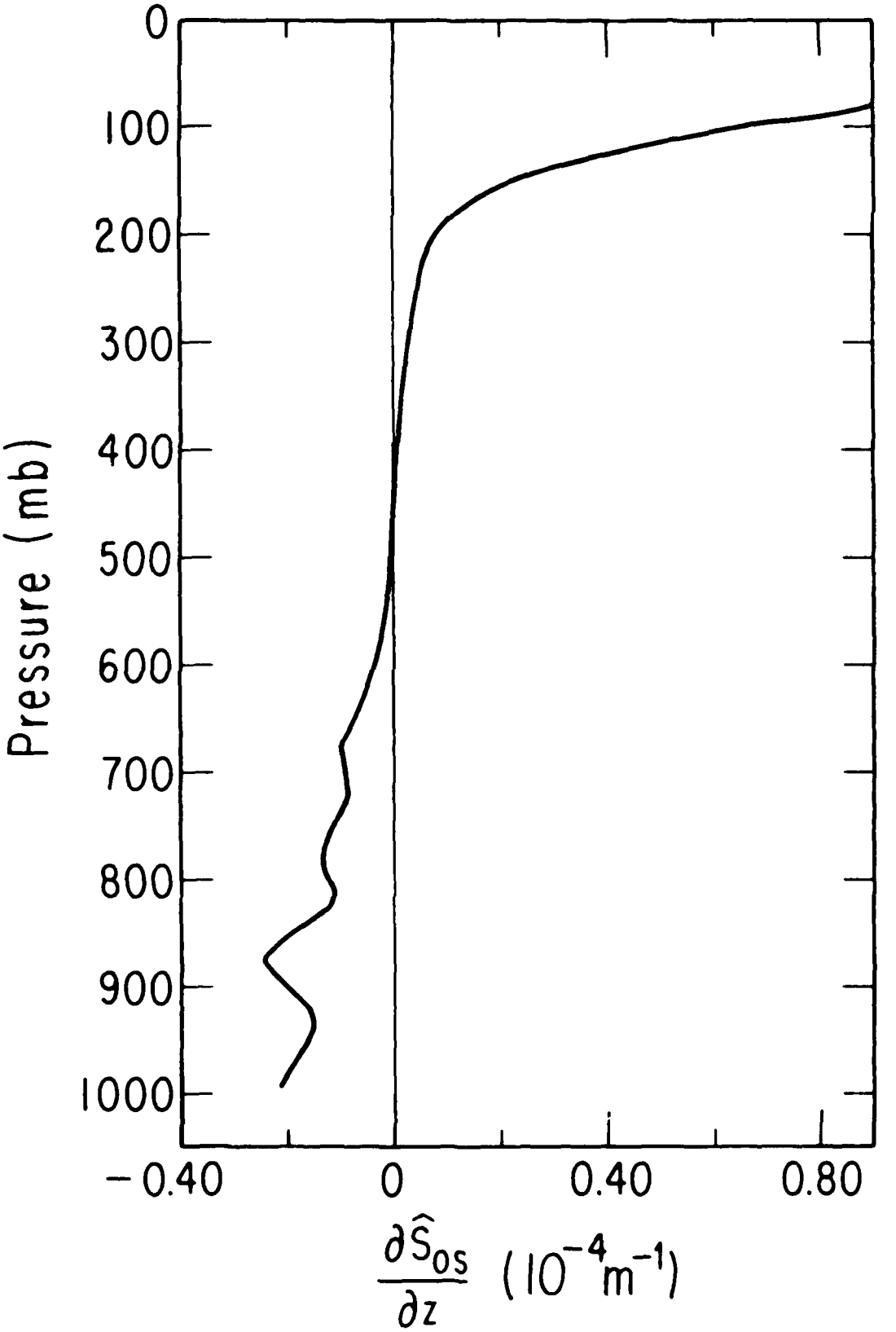
0
100
200
300
400
500
600
700
800
900
1000
Pressure (mb)
-0.40
0
0.40
0.80
$\frac{\partial \hat{S}_{os}}{\partial z}$ $(10^{-4} m^{-1})$

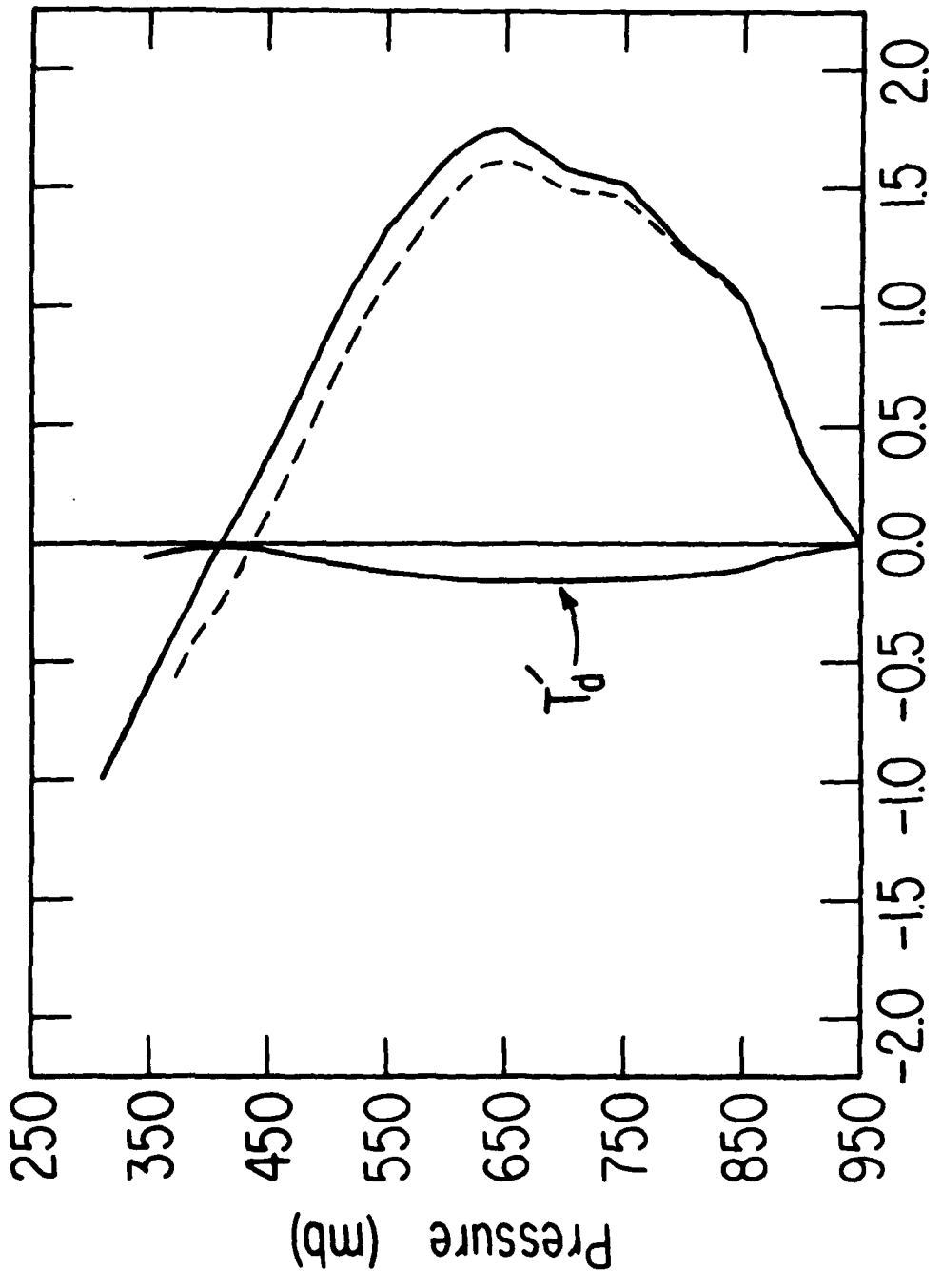
250
350
450
550
650
750
850
950
Pressure (mb)
-2.0
-1.5
-1.0
-0.5
0.0
0.5
1.0
1.5
2.0
$T'_c = T_c - T_o$
T'_d

Figure 3.

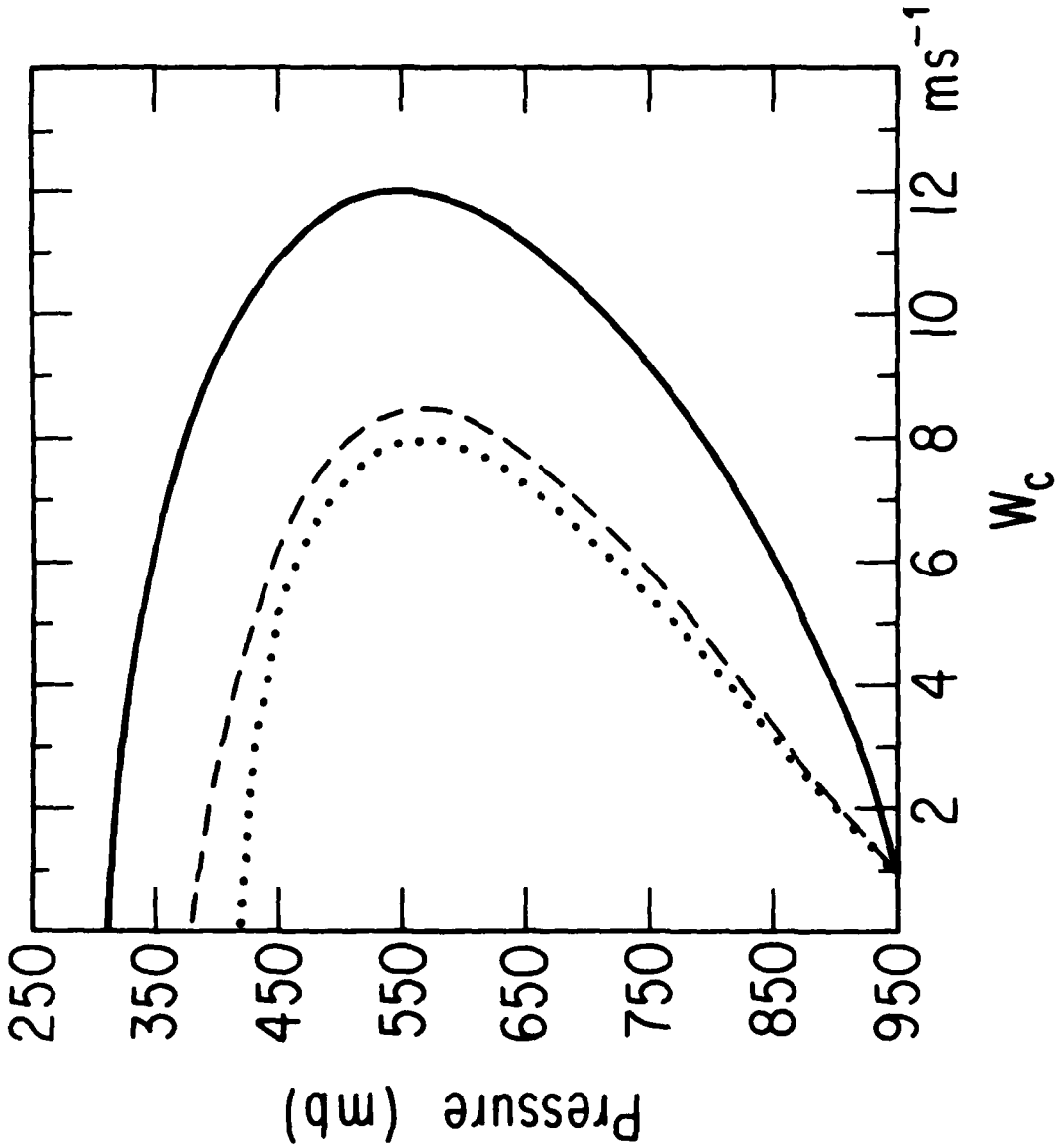

Figure 4.

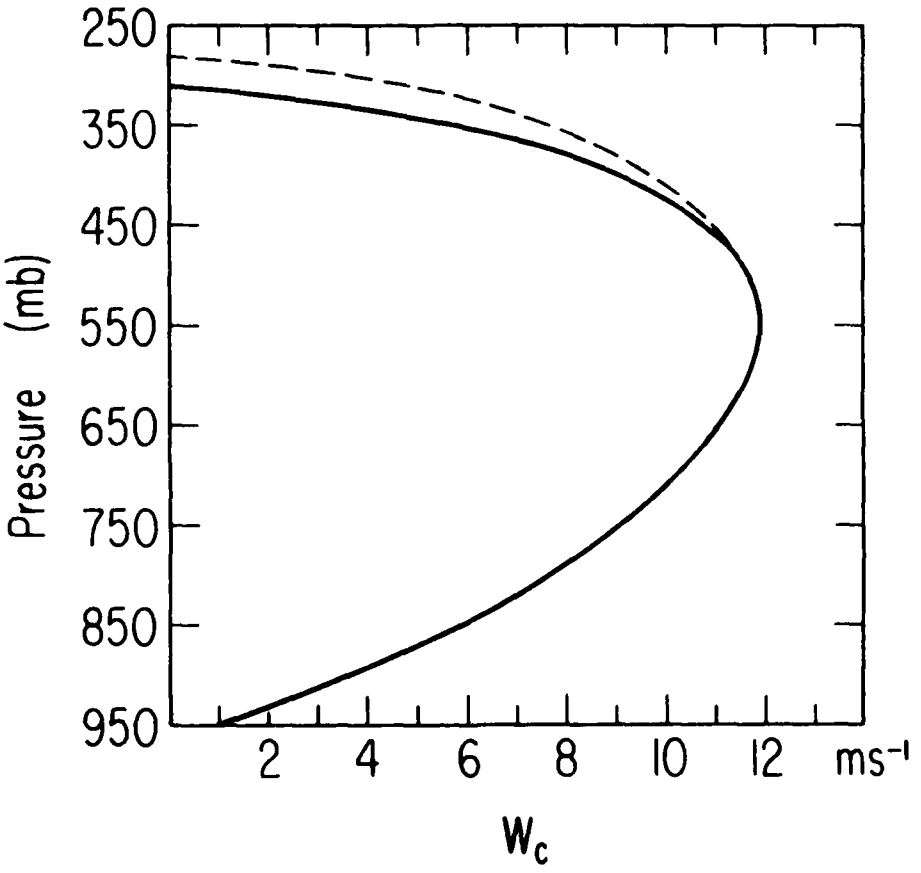

Fig. 5.

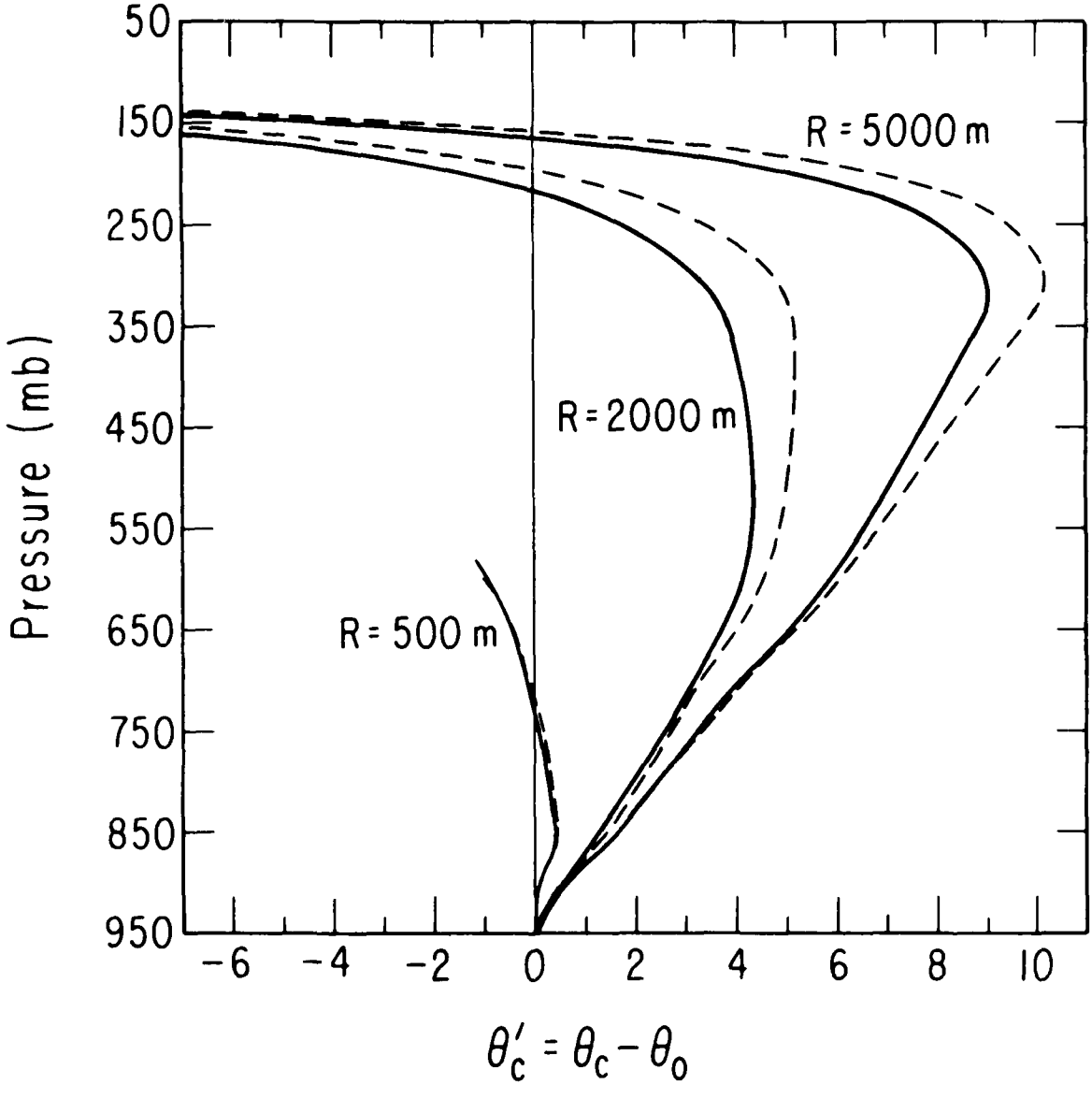
50
150
250
350
450
550
650
750
850
950
Pressure (mb)
R = 5000 m
R = 2000 m
R = 500 m
−6
−4
−2
0
2
4
6
8
10
$\theta'_c = \theta_c - \theta_0$

Fig. 6.

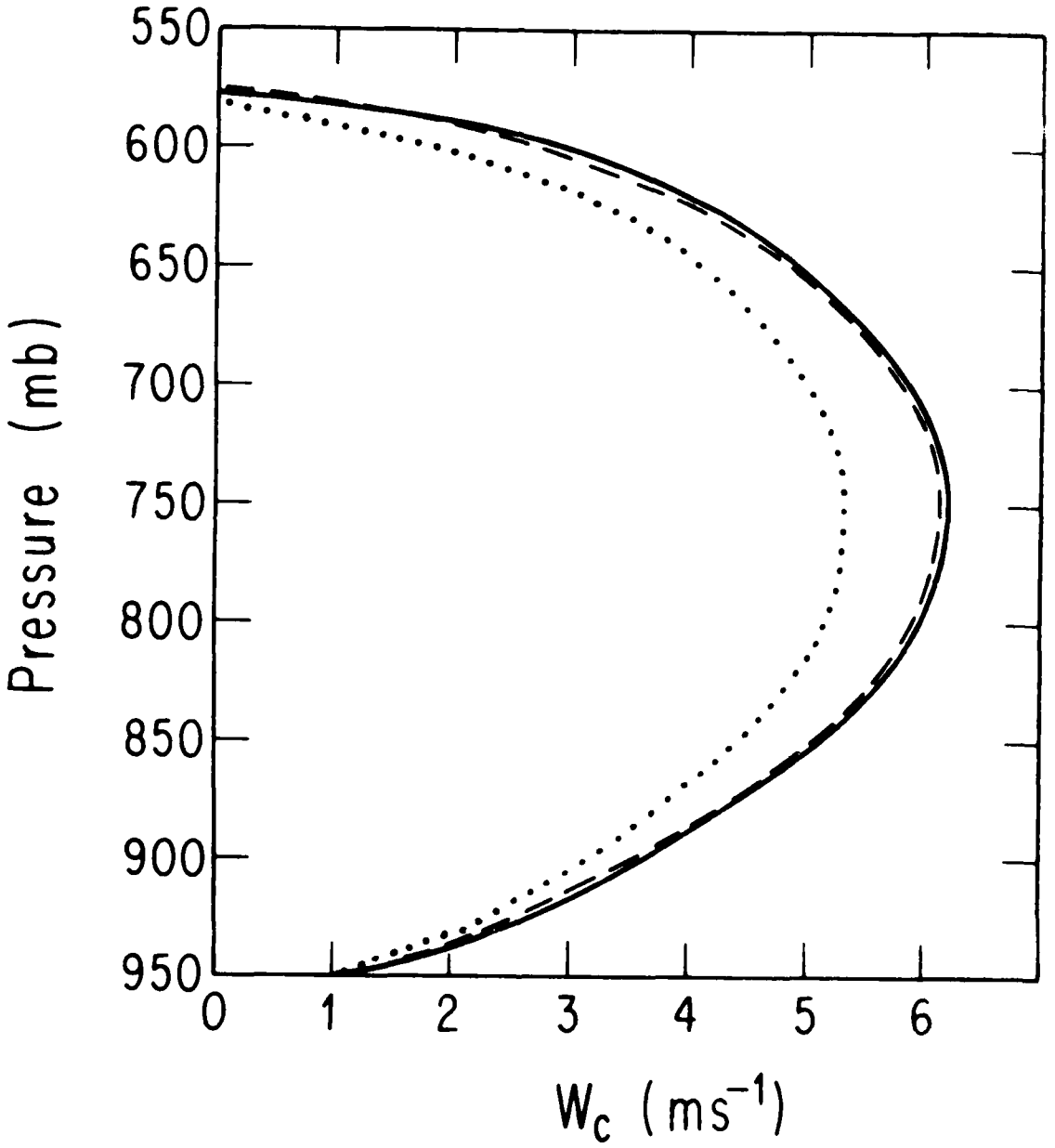

FIG. 7.

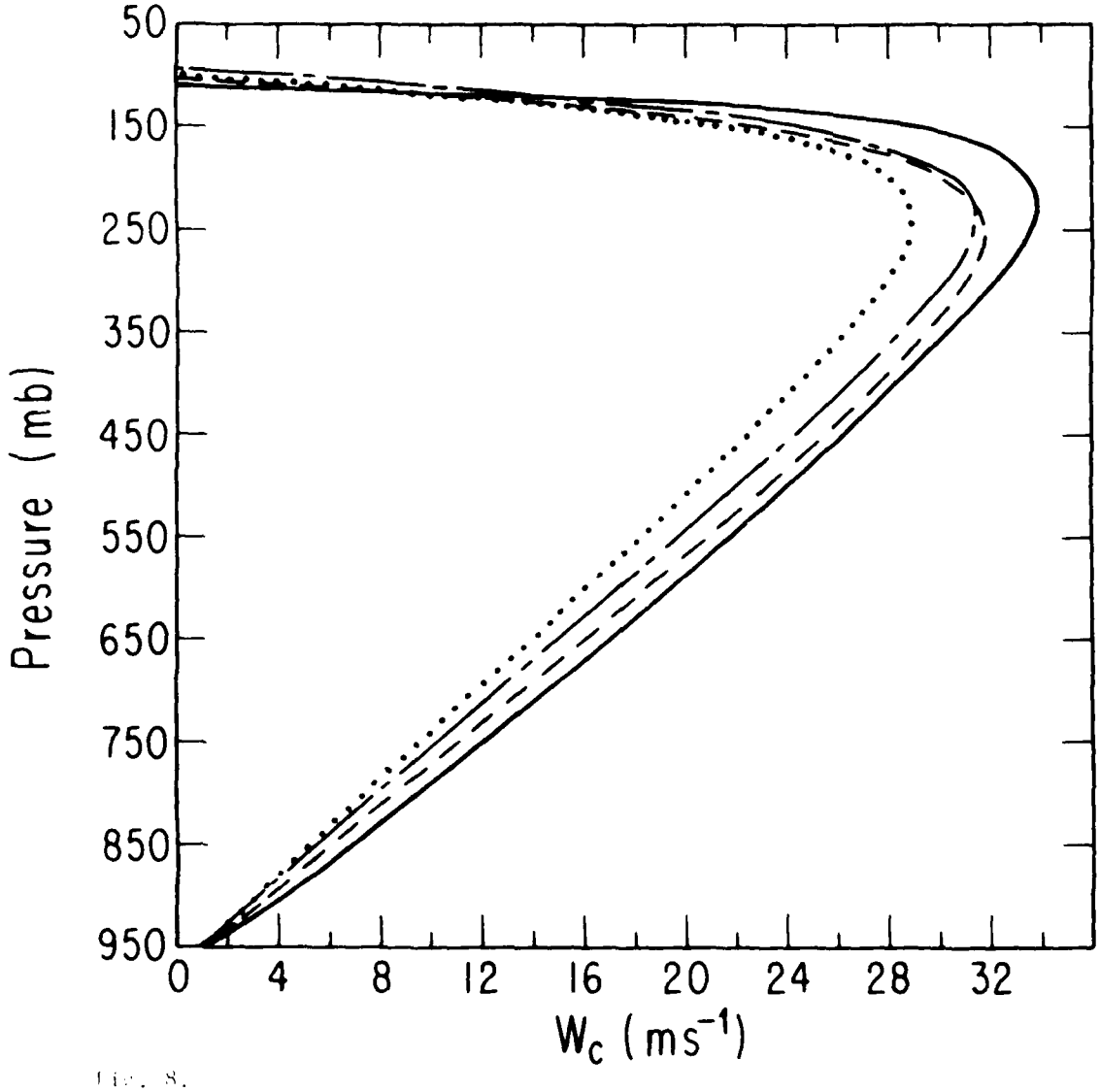
50
150
250
350
450
550
650
750
850
950
Pressure (mb)
0
4
8
12
16
20
24
28
32
W_c (ms^{-1})

FIG. 8.

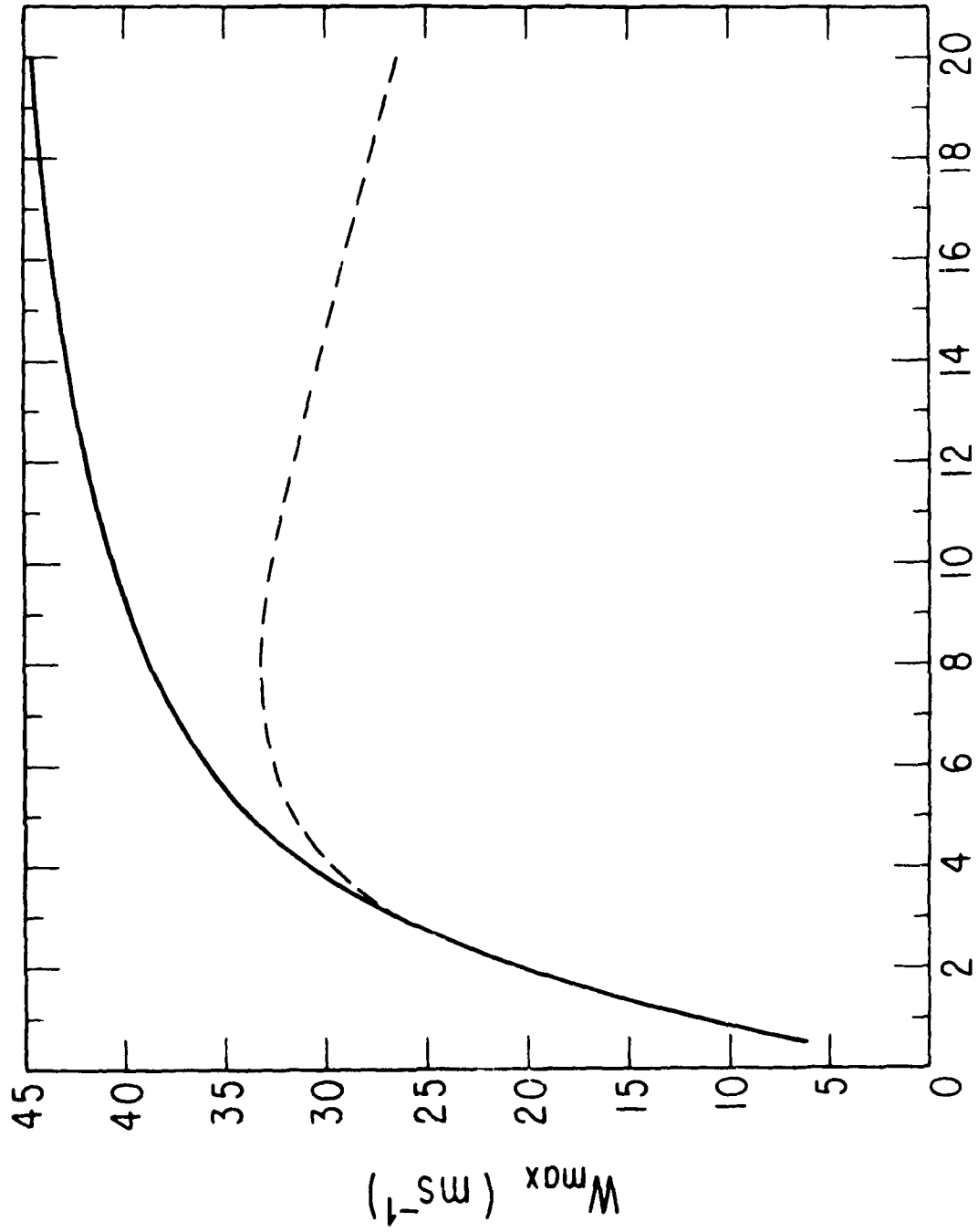
W_{max} (ms^{-1})
45
40
35
30
25
20
15
10
5
0
2
4
6
8
10
12
14
16
18
20
Cloud Radius (km)

FIG. 2.

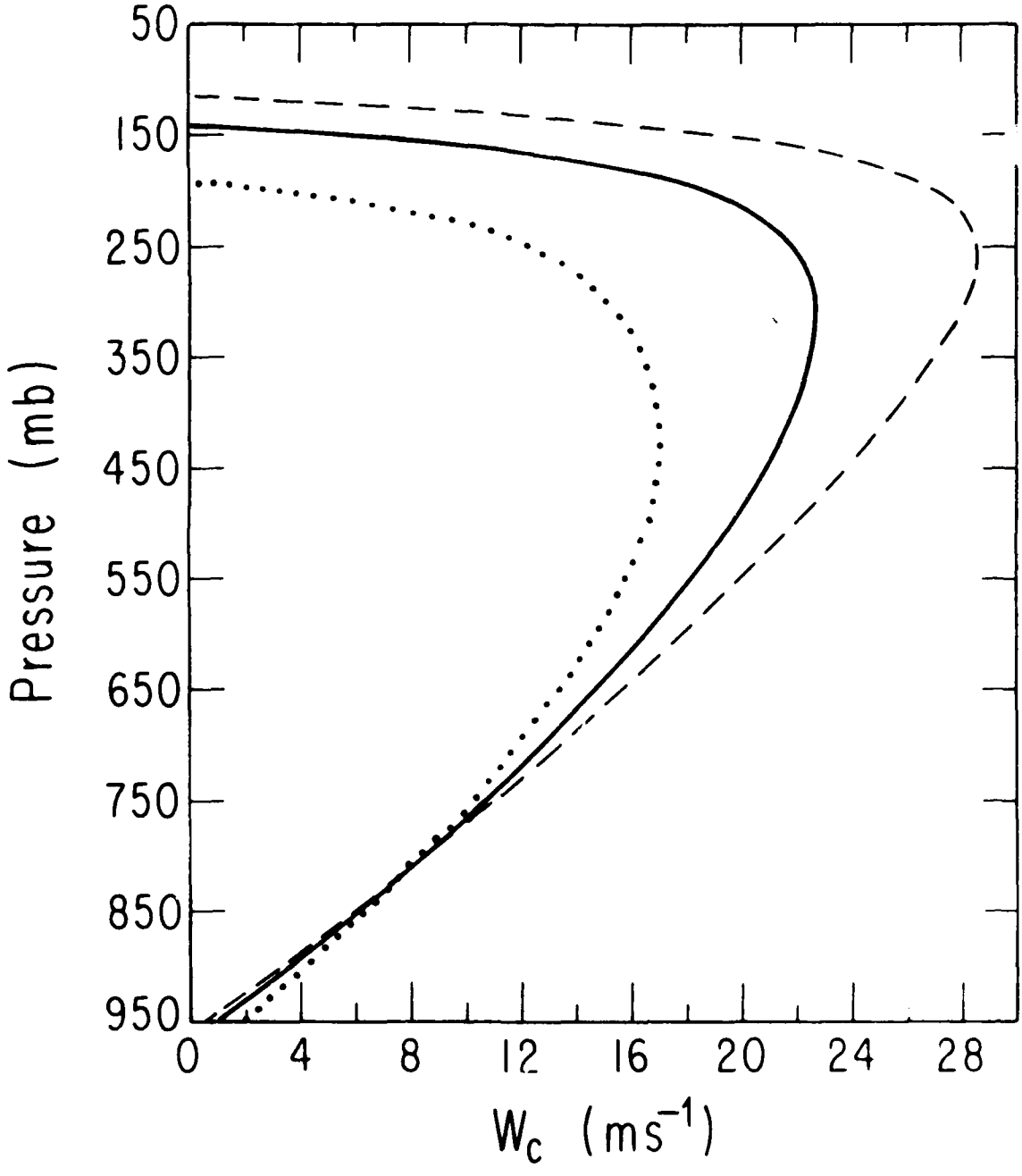
50
150
250
350
450
550
650
750
850
950
Pressure (mb)
0
4
8
12
16
20
24
28
W_c (ms^{-1})

Fig. 10.

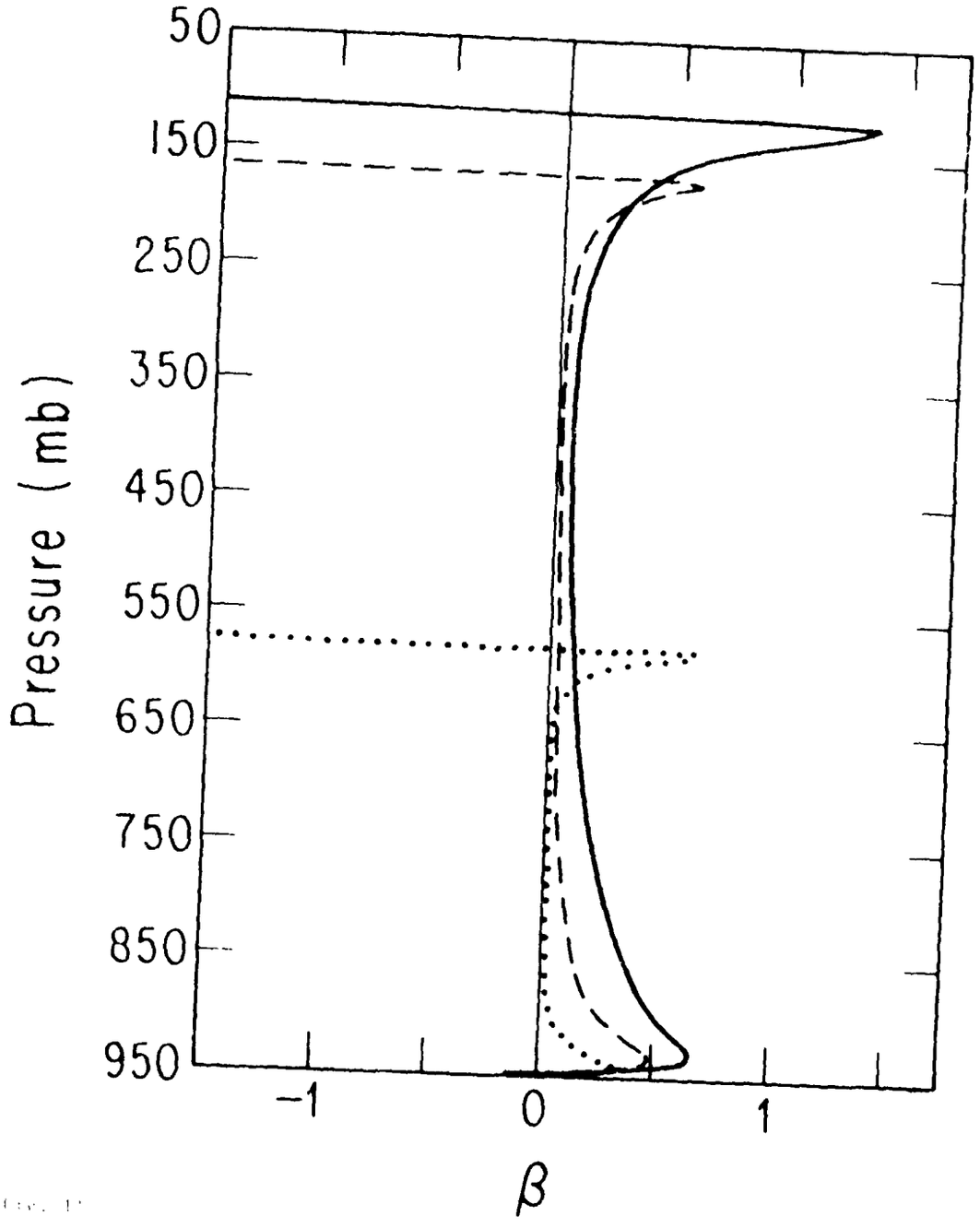
50
150
250
350
450
550
650
750
850
950
Pressure (mb)
−1
0
1
β

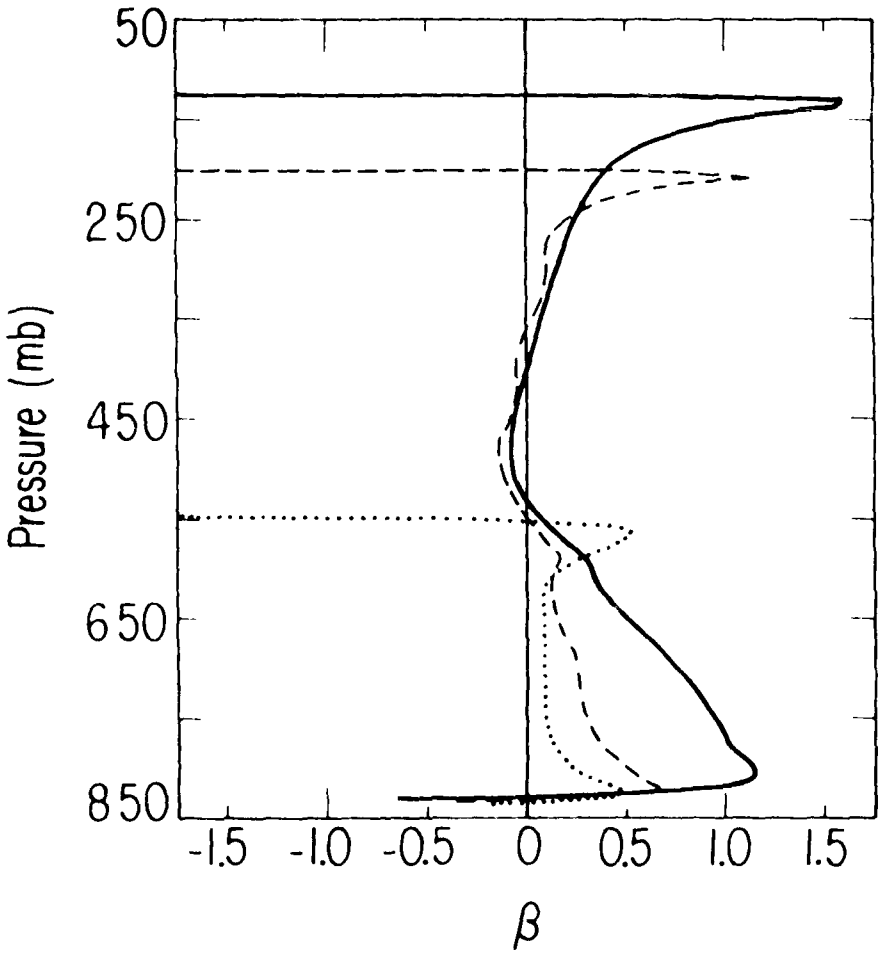

Fig. 12

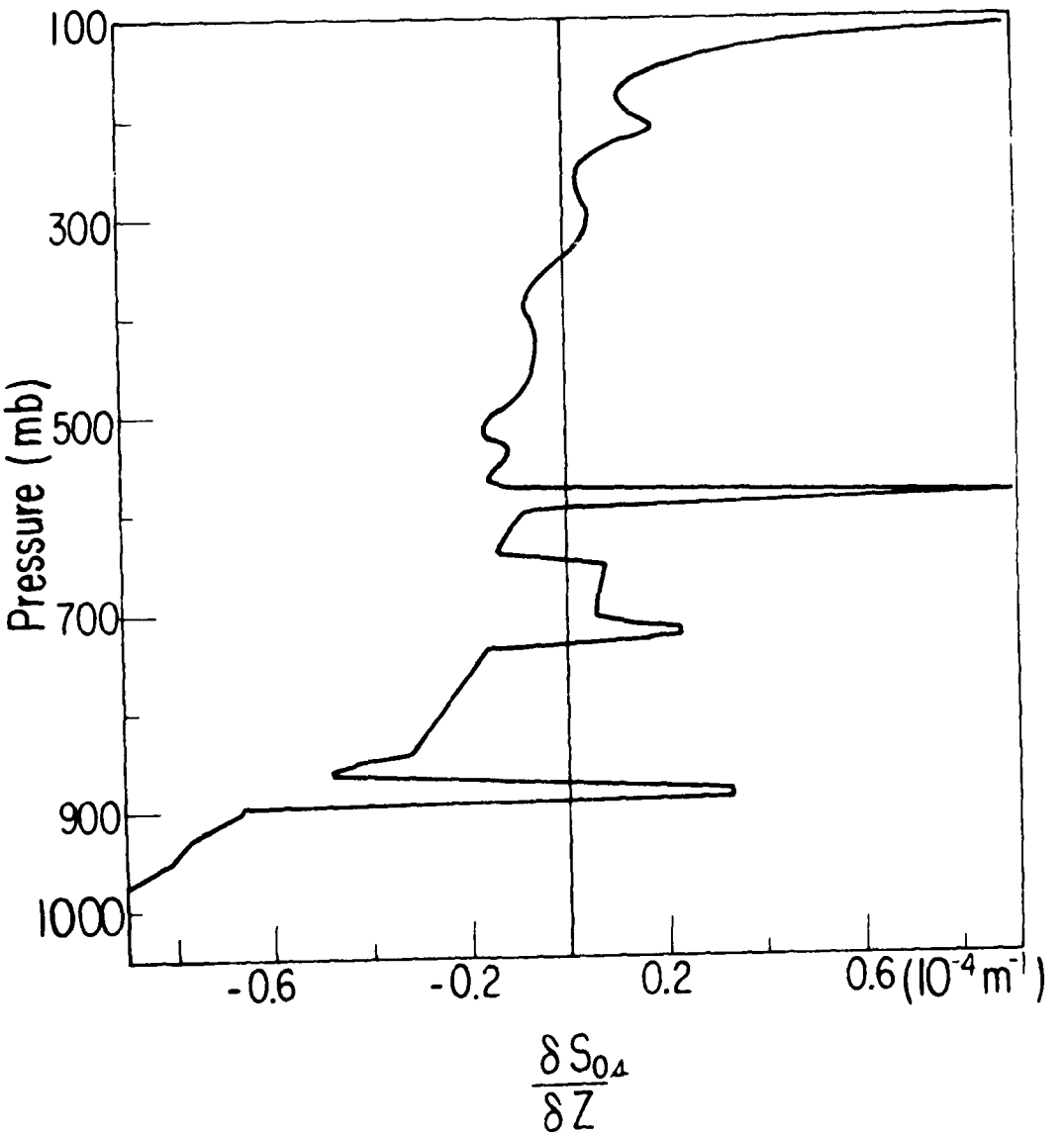

Fig. 13.

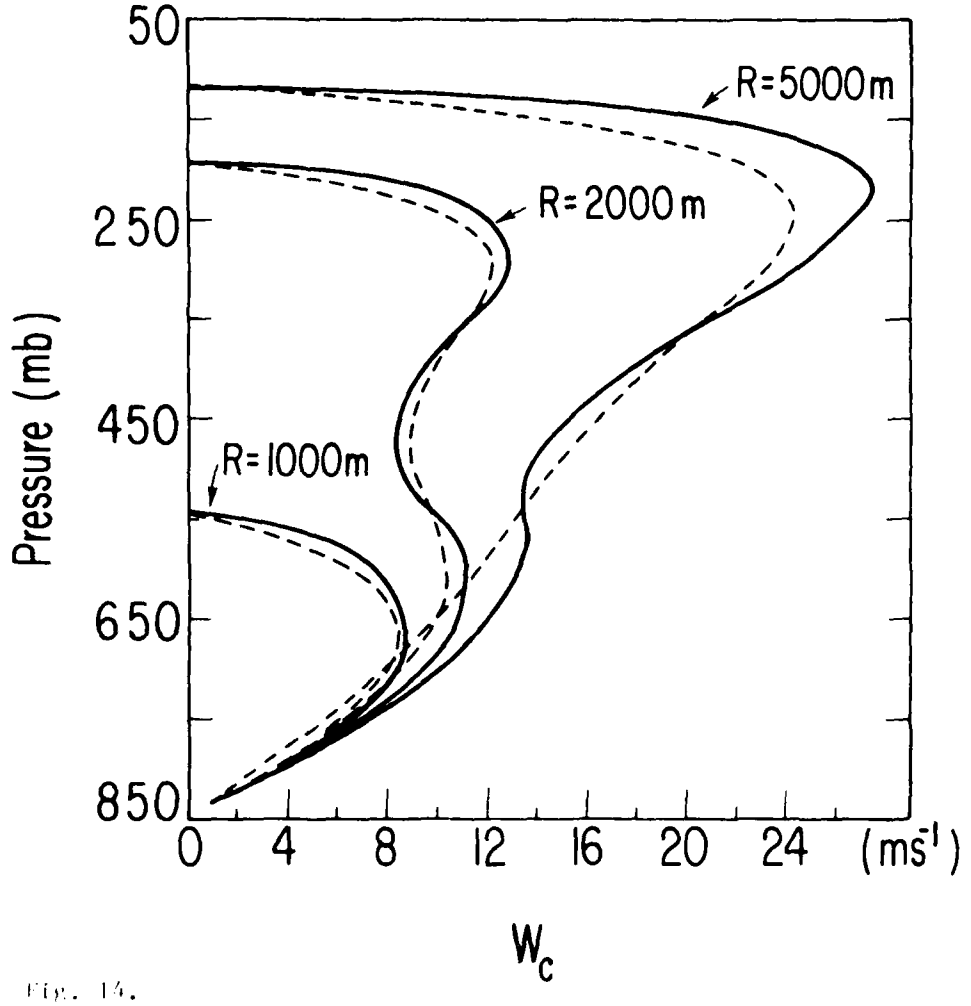
50
250
450
650
850
Pressure (mb)
R=5000m
R=2000m
R=1000m
0
4
8
12
16
20
24
(ms⁻¹)
W_c

Fig. 14.

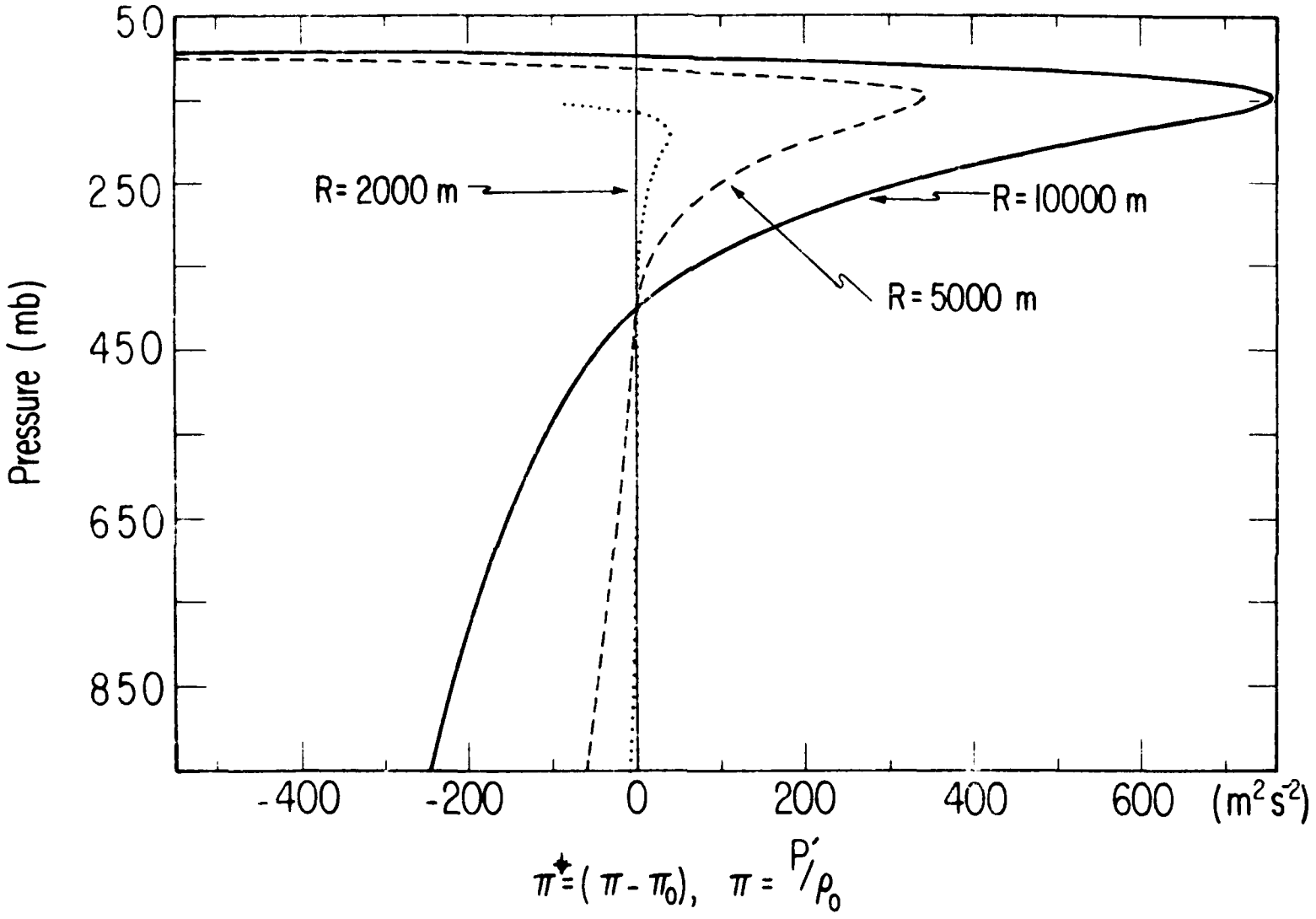
50
250
450
650
850
Pressure (mb)
R= 2000 m
R= 10000 m
R= 5000 m
-400
-200
0
200
400
600
(m² s⁻²)
π* = (π - π₀), π = P'/ρ₀

FIG. 15.

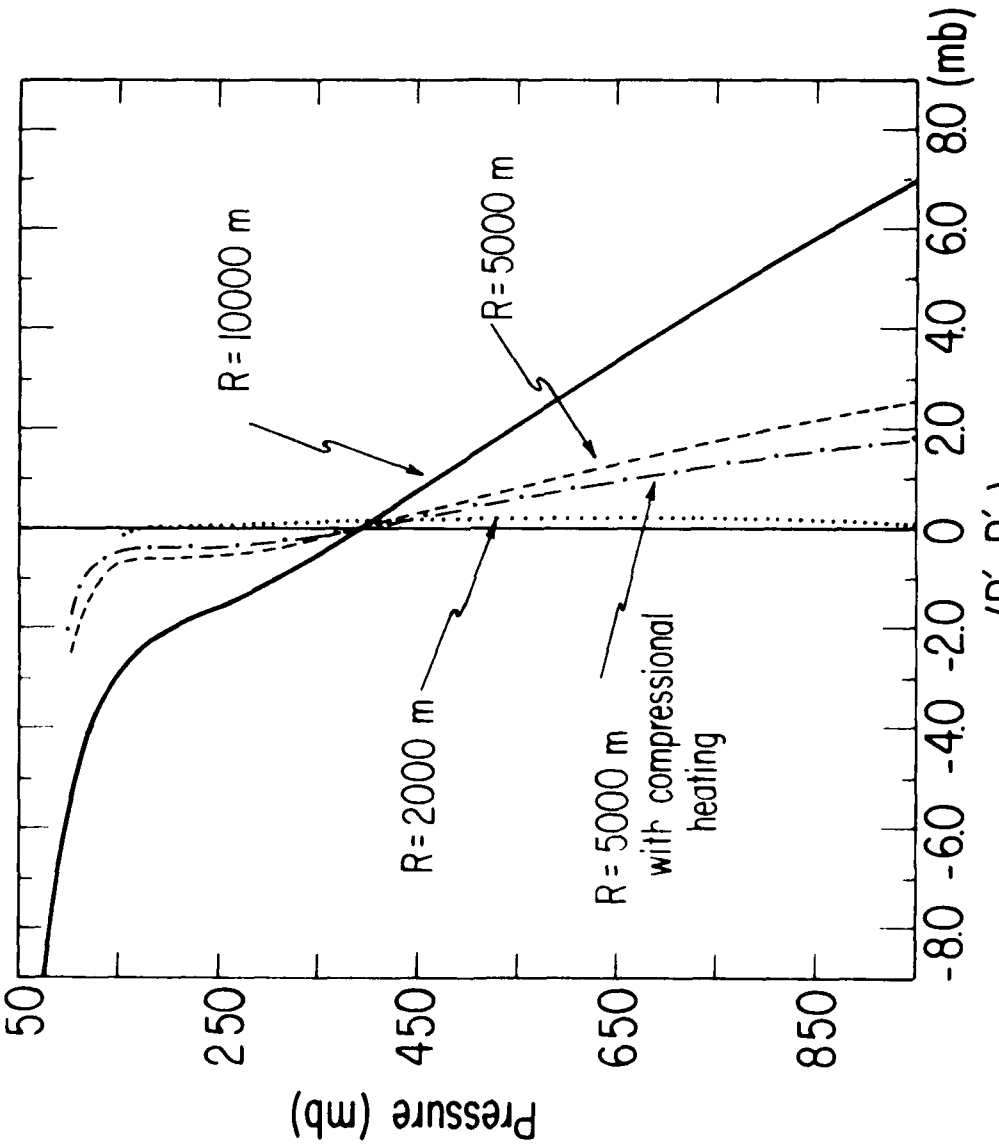
Pressure (mb)
50
250
450
650
850
-8.0 -6.0 -4.0 -2.0 0 2.0 4.0 6.0 8.0 (mb)
(P'- P'o)
R= 10000 m
R= 5000 m
R= 2000 m
R= 5000 m
with compressional
heating

Fig. 14.

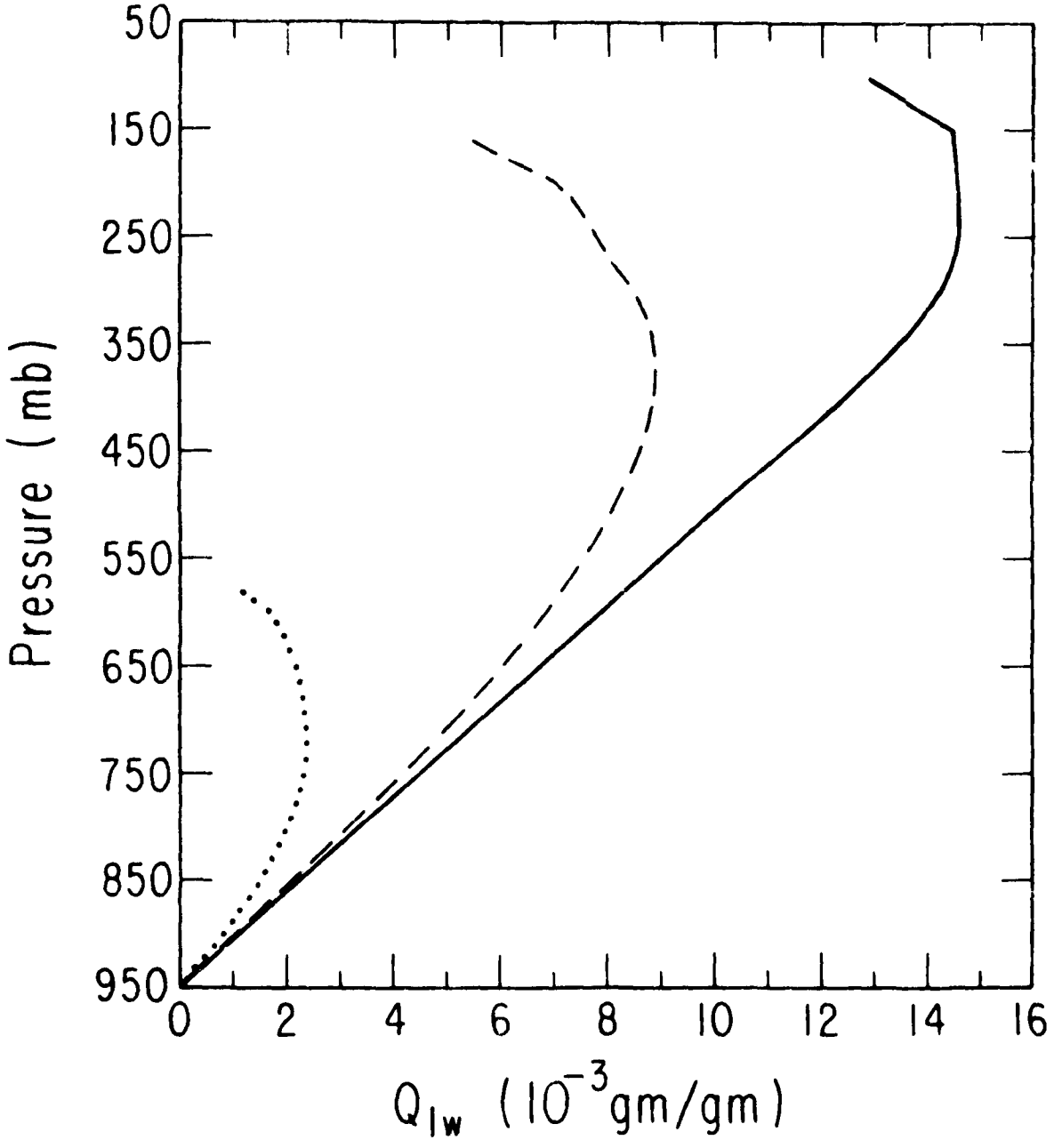
50
150
250
350
450
550
650
750
850
950
Pressure (mb)
0
2
4
6
8
10
12
14
16
Q_{lw} (10^{-3}gm/gm)

Fig. 17.

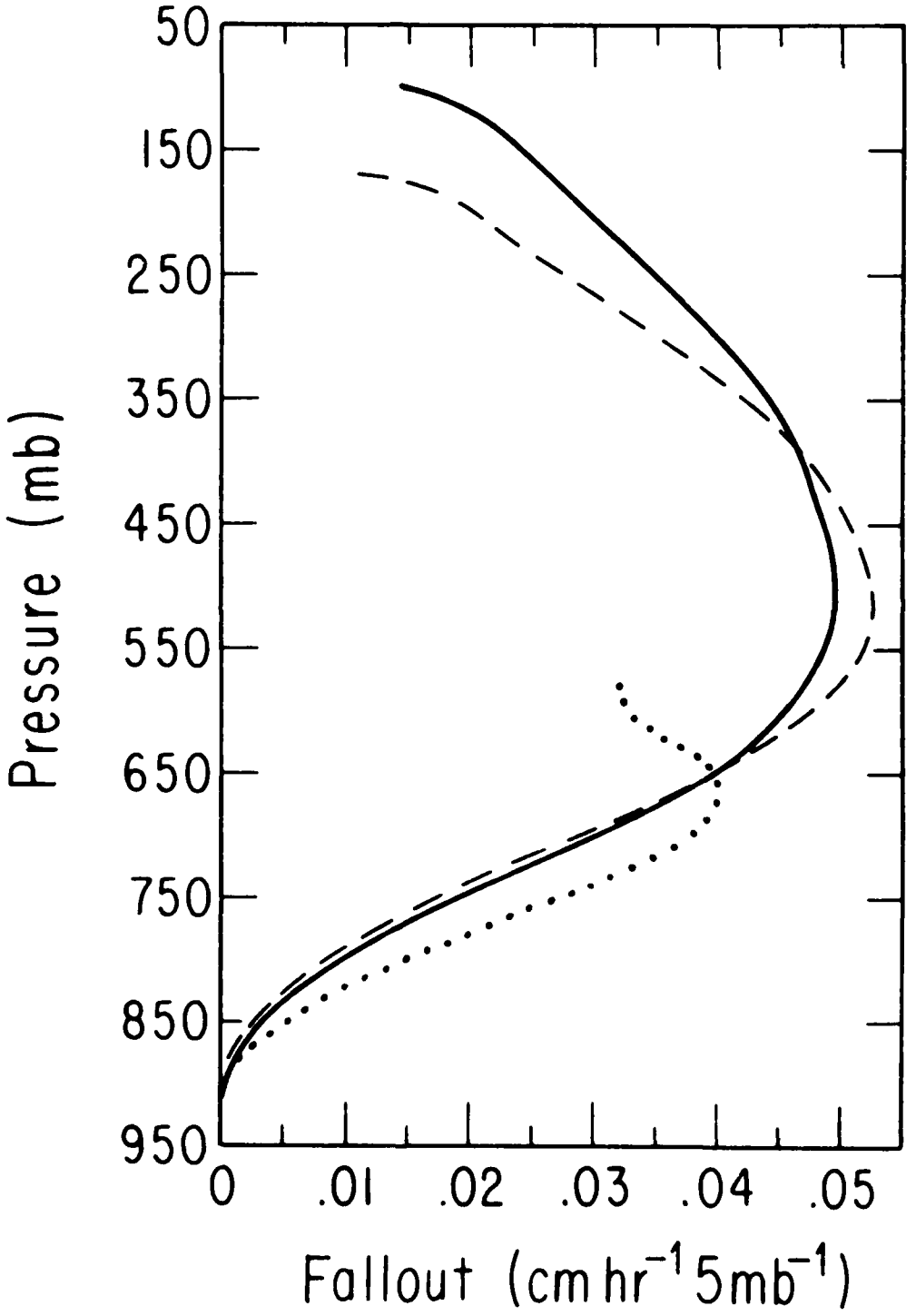
50
150
250
350
450
550
650
750
850
950
Pressure (mb)
0
.01
.02
.03
.04
.05
Fallout (cm hr^{-1} 5mb^{-1})

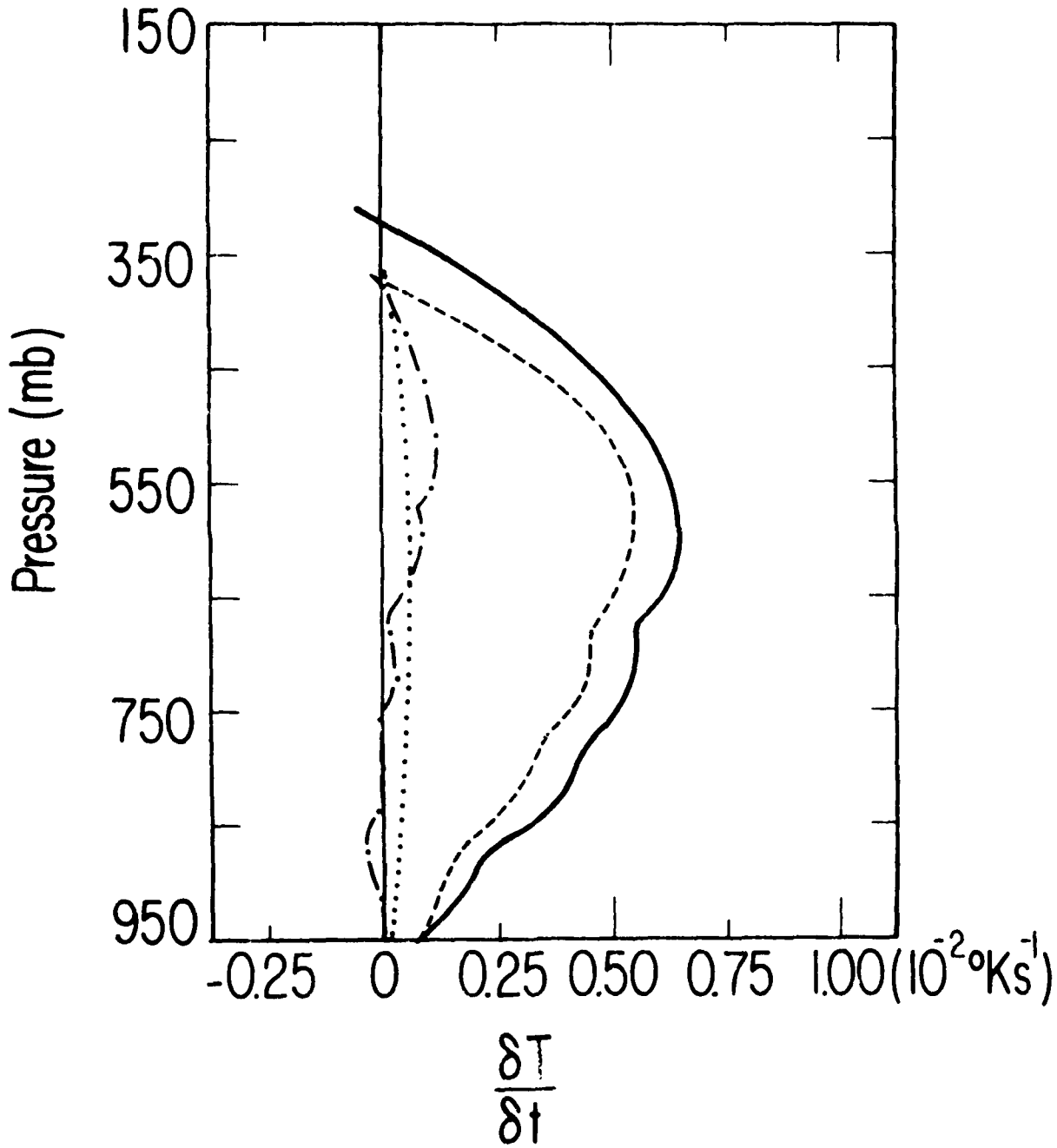
150
350
550
750
950
Pressure (mb)
-0.25
0
0.25
0.50
0.75
1.00
(10⁻² °Ks⁻¹)
δT/δt

Fig. 19.

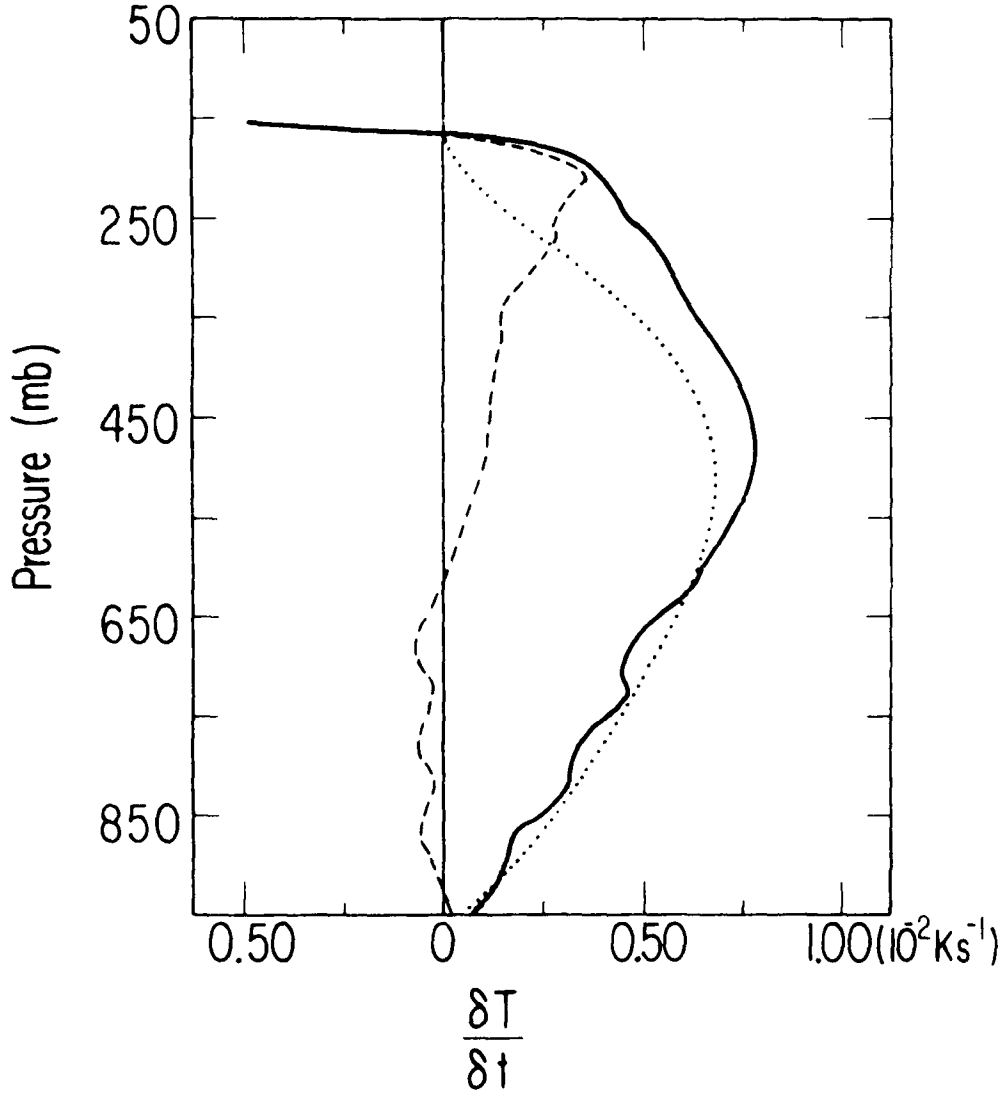

Fig. 20.

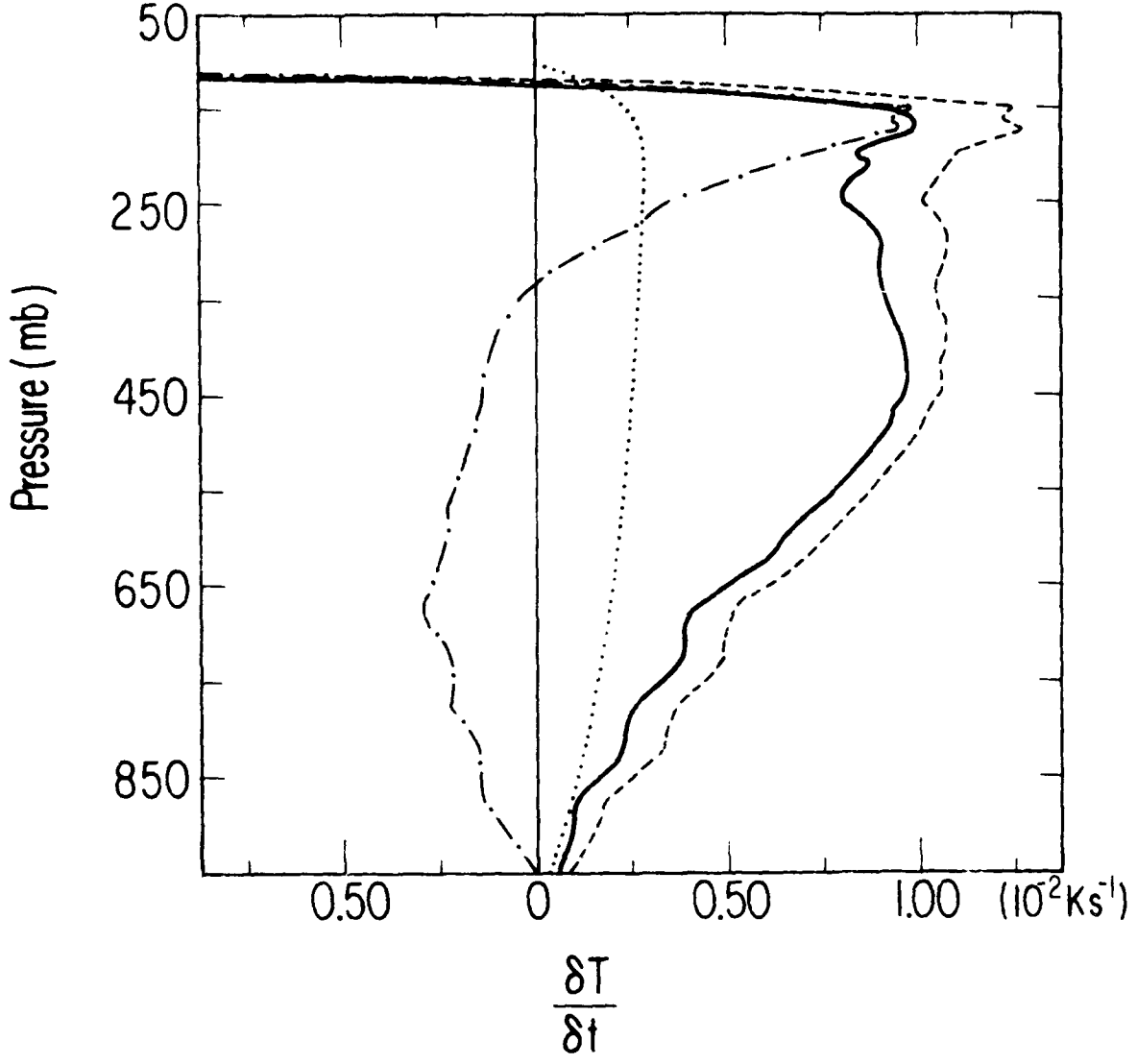
50
250
450
650
850
Pressure (mb)
0.50
0
0.50
1.00
(10⁻²Ks⁻¹)
δT/δt

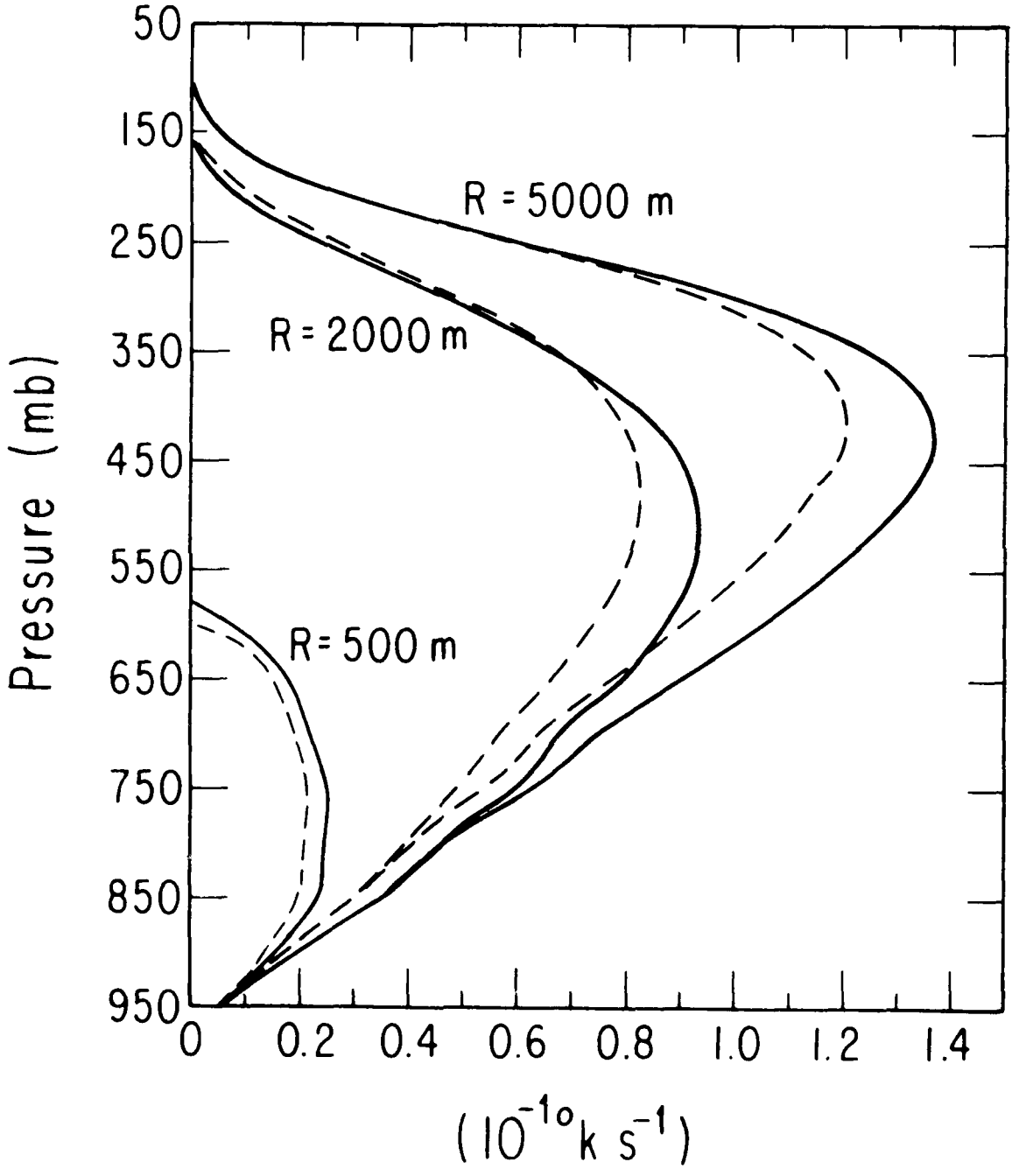
50
150
250
350
450
550
650
750
850
950
Pressure (mb)
R = 5000 m
R = 2000 m
R = 500 m
0
0.2
0.4
0.6
0.8
1.0
1.2
1.4
(10^-10 k s^-1)

Fig. 22.

REFERENCES

Anthes, R. A., 1977: A cumulus parameterization scheme utilizing a one-dimensional cloud model. Mon. Wea. Rev., 105, 270-286.

Hebert, P. J., and C. L. Jordan, 1959: Mean soundings for the Gulf of Mexico area. NHPR No. 30, U. S. Weather Bureau, Miami, Fla., 10 pp. [Available from National Hurricane and Experimental Laboratory, Coral Gables, Fla.]

Holton, J. R., 1973: A one-dimensional cumulus model including pressure perturbation. Mon. Wea. Rev. 101, 201-205.

Johnson, R. H., 1976: The role of convective-scale precipitation downdrafts in cumulus and synoptic-scale interactions. J. Atmos. Sci., 33, 1890-1910.

Kessler, E., 1965: Microphysical parameters in relation to tropical cloud and precipitation distributions and their modifications. Geofis. Intern., 5, 79-88.

____, 1969: On the continuity of water substances in atmospheric circulations. Met. Monographs 10, No. 33, 84 pp.

Kreitzberg, C. W. and D. J. Perkey, 1976: Release of potential instability: Part i. A sequential plume model within a hydrostatic primitive equation model. J. Atmos. Sci., 33, 456-475.

Kuo, H. L., 1965: On formation and intensification of tropical cyclones through latent heat release by cumulus convection. J. Atmos. Sci., 22, 40-63.

____, 1965: Further studies of the properties of cellular convection in a conditionally unstable atmosphere. Tellus, 17, 413-433.

, 1974: Further studies of the parameterization of the influence of cumulus convection on large-scale flow. J. Atmos. Sci., 31, 1232-1240.

Nitta, T., 1978: A diagnostic study of interaction of cumulus updrafts and downdrafts with large-scale motion in GATE. J. Meteor. Soc. Japan, 56, 232-241.

Ogura, Y., and T. Takahashi, 1971: Numerical simulation of the life cycle of a thunderstorm cell., Mon. Wea. Rev., 99, 895-911.

Simpson, J., and V. Wiggert, 1969: Models of precipitating cumulus towers. Mon. Wea. Rev., 97, 471-489.

Squires, P., and J. S. Turner, 1962: An entraining jet model for cumulo-nimbus updraughts. Tellus, 14, 422-434.

Srivastava, R. C., 1967: A study of the effect of precipitation on cumulus dynamics. J. Atmos. Sci., 24, 36-45.

Stommel, H., 1947: Entrainment of air into a cumulus cloud. J. Meteor., 4, 91-94.

Yau, M. K., 1979: Perturbation pressure and cumulus convection. J. Atmos. Sci., 36, 690-694.

Zrnic, D. S., 1978: A dual Doppler variational objective analysis as applied to studies of convective storms. NOAA Technical Memorandum ERL NSSL-85 National Severe Storms Laboratory, Norman, Oklahoma. [Available from National Technical Information Service, Operations Division, Springfield, Va. 22151.]

Zipser, E. J., 1977: Mesoscale and convective scale downdrafts as distinct components of squall-line structure. Mon. Wea. Rev., 105, 1568-1589.

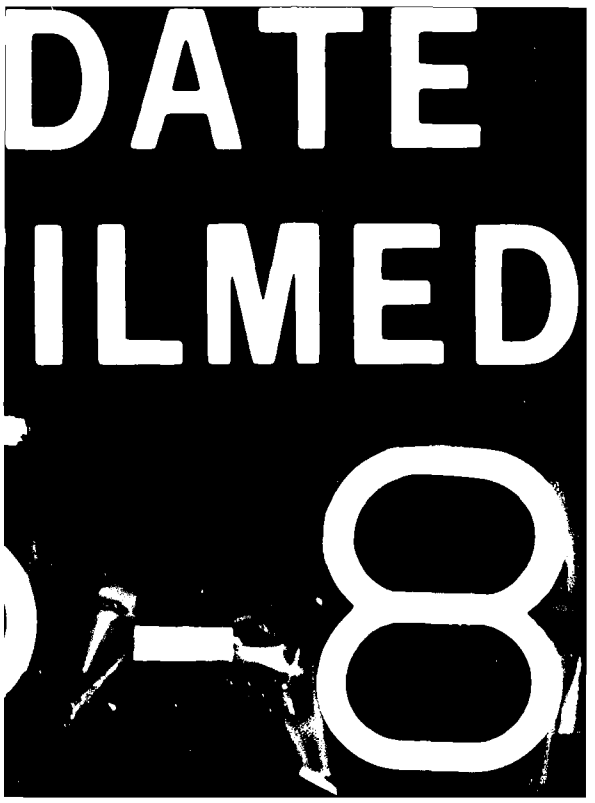
DATE
ILMED
8